Air – snow exchange of nitrate: a modelling approach to investigate physicochemical processes in surface snow at Dome C, Antarctica

Josué Bock[1], Joël Savarino[2,3], and Ghislain Picard[2,3]

[1]Centre for Ocean and Atmospheric Sciences, School of Environmental Sciences, University of East Anglia, Norwich Research Park, Norfolk, NR4 7TJ, Norwich, UK
[2]Université Grenoble Alpes, Laboratoire de Glaciologie et Géophysique de l'Environnement (LGGE), 38041 Grenoble, France
[3]CNRS, LGGE UMR5183, 38041 Grenoble, France

Correspondence to: Josué Bock (j.bock@uea.ac.uk)

Abstract. Snowpack is a multiphase (photo)chemical reactor that strongly influences the air composition in polar and snow-covered regions. Snowpack plays a special role in the nitrogen cycle, as it has been shown that nitrate undergoes numerous recycling stages (including photolysis) in the snow before being permanently buried in the ice. However, the current understanding of these

5   physicochemical processes remains very poor. Several modelling studies have attempted to reproduce (photo)chemical reactions inside snow grains, but these required strong assumptions to characterise snow reactive properties, which are not well defined. Air – snow exchange processes such as adsorption, solid state diffusion or co-condensation also affect snow chemical composition. Here, we present a model including a physically based parameterisation of these processes for nitrate. Using as

10   input a one-year long time series of atmospheric nitrate concentration measured at Dome C, Antarctica, our process-resolving model reproduces with good agreement the nitrate concentration measured in surface snow. By investigating the relative importance of the main exchange processes, this study shows that, on the one hand, the combination of bulk diffusion and co-condensation incorporation processes allows a good reproduction of the measurements (correlation coefficient $r = 0.95$),

15   with a correct amplitude and timing of summer peak concentration of nitrate in snow. During winter, nitrate concentration in surface snow is mainly driven by thermodynamic equilibrium, whilst the peak observed in summer is explained by the kinetic process of co-condensation. On the other hand, the adsorption of nitric acid on the surface of the snow grains, constrained by an already existing parameterisation for the isotherm, fails to fit the observed variations. During winter and spring, the

20   modelled adsorbed concentration of nitrate is 2.5 and 8.3-fold higher than the measured one, respectively. A strong diurnal variation driven by the temperature cycle and a peak occurring in early spring are two other major features that do not match the measurements. This study clearly demonstrates that co-condensation is the most important process to explain nitrate incorporation in snow undergoing temperature gradient metamorphism. The parameterisation developed for this process can now

25 be used as a foundation piece in snowpack models to predict the inter-relationship between snow physical evolution and snow nitrate chemistry.

1 Introduction

The nitrogen cycle governs atmospheric oxidants budget through the photochemistry of nitrogen oxides ($NO_x = NO + NO_2$) which are strongly coupled with ozone (O_3) and hydroxyl (OH) chem-
30 istry in the troposphere (Seinfeld and Pandis, 1998; Finlayson-Pitts and Pitts, 2000). Atmospheric nitrate is the end product of NO_x oxidation, and the snowpack (and subsequently the firn and ice) acts as a sink for it. Temporal variations of the nitrate concentration recorded in ice cores (Legrand and Mayewski, 1997) could thus provide information about the oxidative capacity of the atmosphere in past times (Dibb et al., 1998), or even about past solar activity (Traversi et al., 2012). However,
35 as illustrated by Davis et al. (2008, Fig. 2), several post-deposition processes occur in the snow and hamper our current ability to interpret ice core records of nitrate. As a first evidence of such post-deposition processes, NO_x has been shown to be produced in sunlit snowpack (Honrath et al., 1999, 2000b, 2002; Jones et al., 2000; Beine et al., 2002), with a production pathway involving nitrate photolysis in snow rapidly elucidated afterwards (Jones et al., 2000; Dibb et al., 2002; Hon-
40 rath et al., 2002). These pioneering works drove numerous field campaigns (e.g. SNOW99 (Honrath et al., 2000b), ISCAT2000 (Davis et al., 2004), ANTCI (Eisele et al., 2008), CHABLIS (Jones et al., 2008), OPALE (Preunkert et al., 2012)), as well as laboratory studies (Honrath et al., 2000a; Dubowski et al., 2001, 2002; Chu and Anastasio, 2003, 2007; Cotter et al., 2003; Zhu et al., 2010; Meusinger et al., 2014; Berhanu et al., 2014) and modelling studies (Jacobi and Hilker, 2007; Boxe
45 and Saiz-Lopez, 2008; Liao and Tan, 2008; Bock and Jacobi, 2010; Thomas et al., 2011; Toyota et al., 2014; Erbland et al., 2015; Murray et al., 2015) in order to improve the understanding of the underlying processes responsible for the nitrogen recycling inside the snowpack. These studies focused on the nitrate photolysis in the photic zone of the snowpack and the subsequent release of NO_x to the overlying atmosphere. However, none of these studies investigated the physicochemical incor-
50 poration processes of atmospheric nitrate into snow. Yet, it is now well documented that the nitrate concentration in the surface snow exhibits a seasonal peak during summer on the Antarctic plateau (Erbland et al., 2013, and ref. therein), when the solar flux is close to its annual maximum and photolysis is strongest. This implies that some incorporation processes counteract photochemical loss, and thus need to be studied in order to understand the nitrate budget of the snow. In a recent study
55 from Jones and co-workers, measurements of gaseous HNO_3 were carried out with a high temporal resolution of 10 min, during 4 winter months at Halley station, located at coastal Antarctica (Jones et al., 2014). This work reveals that HNO_3 concentration is highly correlated with the temperature, highlighting that physical air–snow exchange processes play a key role during this period of the year.

Numerous experimental studies of adsorption on ice surfaces have demonstrated that several chemical compounds, and especially acidic gases such as HCl and HNO_3, have a great affinity for ice surface (see reviews by Abbatt, 2003; Huthwelker et al., 2006). Other post-deposition physical processes also affect snow chemical composition (Dominé et al., 2008). Several small molecules, such as HCl (Dominé et al., 1994; Thibert and Dominé, 1997), HNO_3 (Thibert and Dominé, 1998), HCHO (Perrier et al., 2003; Barret et al., 2011b) and H_2O_2 (Sigg et al. (1992) and ref. therein; Conklin et al. (1993); Jacob and Klockow (1993); McConnell et al. (1997b)) form solid solutions in ice. Other species such as SO_2 (Clapsaddle and Lamb, 1989; Conklin and Bales, 1993; Huthwelker et al., 2001) and HONO (Pinzer et al., 2010; Kerbrat et al., 2010) may also diffuse into bulk ice. Thus, solid state diffusion is either able to bury these molecules in the inner parts of snow crystals, or on the contrary to make it available for surface (photo)chemical reactions after migration from the bulk crystal to its surface.

Another physical process, known as co-condensation, is the simultaneous condensation of water vapour and trace gases at the air–ice interface. Water vapour fluxes in the snowpack are mainly driven by temperature gradients, leading to massive mass transfer from the warmest snow layers which sublimate, towards the coldest parts where vapour condensates (Calonne et al., 2014; Ebner et al., 2015; Hansen and Foslien, 2015). More generally, the subsequent change in snow morphology, called temperature gradient metamorphism, affects the whole snowpack following seasonal temperature variations (Marbouty, 1980; Sommerfeld, 1983; Flin and Brzoska, 2008; Pinzer and Schneebeli, 2009; Pinzer et al., 2012; Ebner et al., 2015), and particularly the upper part of the snowpack subjected to the diurnal temperature cycles (Picard et al., 2012; Champollion et al., 2013, and ref. therein). Indeed, high crystal growth rates are observed at the surface of the snowpack, and at about 10 cm under the snow surface (Colbeck, 1989, Fig. 8) though the exact depth is subject to debate (Kuipers Munneke et al., 2009; Libois et al., 2014). Along with the vapour flux, trace impurities present in the interstitial air, or temporarily adsorbed on the ice surface, might be incorporated inside the crystals (Conklin et al., 1993; Bales et al., 1995; Dominé and Thibert, 1996; Xueref and Dominé, 2003; Dominé and Rauzy, 2004; Kärcher and Basko, 2004; Ullerstam and Abbatt, 2005; Kärcher et al., 2009). This kinetic process of incorporation is much more efficient than air–ice thermodynamic equilibrium, which probably explains why measured concentrations have sometimes been shown to be of out of equilibrium (Bales et al., 1995; Dominé and Thibert, 1995, 1996; Ullerstam and Abbatt, 2005).

The models of snow chemistry developed so far focus on snow-to-air processes driven by (photo)chemistry, since they mainly intend to reproduce field measurements of NO_x fluxes emitted by the snowpack. Recent work from Erbland et al. (2013, 2015) indeed suggests that the denitrification of the snowpack by means of physical release is negligible compared to the photochemical processes. Thus, air-to-snow physical exchange processes were ignored in several studies (Boxe and Saiz-Lopez, 2008; Bock and Jacobi, 2010). In other models, these processes were bypassed through ad-hoc parameterisation and/or implemented using air–liquid equilibrium following Henry's law, based on the

3

assumption that snow crystals are covered by a liquid layer (Liao and Tan, 2008; Thomas et al., 2011; Toyota et al., 2014). Such modelling approaches and their pitfalls were discussed in detail by Dominé et al. (2013). As far as we are aware, the only physically based modelling studies of air–snow exchange processes were carried out in the late 1990's to interpret multiyear firn concentration profiles of H_2O_2 (McConnell et al., 1997a, b, 1998) and of HCHO (Hutterli et al., 1999, 2002). As summarised by Hutterli et al. (2003, Fig. 1), both of these series of modelling studies handled air-snow uptake/release through an exchange coefficient accounting for an Henry's law type partitioning between the two compartments, but did not included the co-condensation process nor the solid state diffusion inside the ice crystals. More recently, Barret et al. (2011a) proposed an air–snow exchange model to reproduce surface snow HCHO concentration. In that study, the surface snow is depicted as a unique spherical, layered grain whose surface concentration of HCHO is constrained by the air–ice thermodynamic equilibrium. Their model uses as input the measured gas phase HCHO concentration and solves the spherical diffusion equation with radial symmetry to calculate the mean concentration in the whole snow grain. Their results reproduce the concentration measured in surface snow during a 36-hour intensive sampling period in the course of OASIS 2009 campaign with fairly good agreement (Barret et al., 2011a, Fig. 4).

For the first time, we propose a process-resolving model for air–snow exchange of nitric acid (HNO_3), which allows an investigation of the above mentioned physicochemical exchange processes. Following a similar approach to that of Barret et al. (2011a), we developed a model considering a single spherical layered snow grain. This snow grain is assumed to be in direct contact with the air just above the snowpack. Using the atmospheric nitrate concentration measured at Dome C (DC) for about one year as input, the model calculates the snow nitrate concentration resulting from (i) adsorption on the snow grain surface, (ii) solubilisation into the outermost layer according to thermodynamic equilibrium and diffusion inside the snow grain, and (iii) co-condensation following vapour fluxes inside the upper snowpack. Model results are compared to nitrate concentration in the uppermost ~ 4 mm of the snowpack ("skin layer" hereinafter).

The input datasets are presented in the next section, and the model is described in Sect. 3. The results obtained in configuration 1 (adsorption only) are presented and discussed in Sect. 4, and those relative to the model configuration 2 (solid state diffusion) are presented in Sect. 5.

2 Input data description

2.1 Annual atmospheric and skin layer nitrate concentrations at Dome C

2.1.1 Atmospheric nitrate

Atmospheric nitrate, which includes both particulate nitrate and gaseous HNO_3, was measured continuously at DC between January 2009 and January 2010 using a high-volume air sampler placed

4

130 5 m above the snow surface (Erbland et al., 2013). Atmospheric nitrate was collected on glass fibre filters, which efficiently trap both particulate nitrate and gaseous HNO_3 (Frey et al., 2009; Erbland et al., 2013). Atmospheric nitrate was quantitatively extracted in 40 cm^3 of ultrapure water via centrifugation using Millipore Centricon™ filter units, and its concentration was then determined using the colorimetric method as described in Erbland et al. (2013). Atmospheric nitrate concentration was

135 calculated as the ratio of the total NO_3^- filter loading to the total volume of air pumped through the filter at STP conditions and expressed in $ng\,m^{-3}$.

Atmospheric nitrate samples were collected for 37 separate 5–7 day periods (see Fig. 1a). Over the year, 10 samples were dedicated to ^{35}S measurement. The missing values were linearly interpolated hereafter (dashed lines in Fig. 1a). As can be seen in Fig. 1a, atmospheric nitrate concentration is low

140 and steady, with a mean value of $(8.2 \pm 5.1)\,ng\,m^{-3}$ from March to September, followed by a sharp increase during the spring (average value of $(98.5 \pm 39.7)\,ng\,m^{-3}$ from October to December, with peak values greater than $130\,ng\,m^{-3}$). A rapid decrease is observed in early summer. This yearly pattern is in good agreement with previous measurements performed at DC between January 2007 and January 2008 (Frey et al., 2009).

145 A few simultaneous measurements of atmospheric nitrate (also reported as "filterable nitrate", $f-NO_3^-$) and HNO_3 give further insight into the partitioning between both. Arimoto et al. (2008, Fig. 5) and Davis et al. (2008, Fig. 3) report concurrent measurements of $f-NO_3^-$ and HNO_3 carried out during 23 days in the course of the ANTCI campaign, at South Pole. Atmospheric nitrate was measured in a very similar way as at DC, using a high-volume air sampler with Whatman 41™ filters

150 which have been shown to efficiently collect atmospheric nitrate as well (Arimoto et al., 2008, and ref. therein). This dataset reveals that HNO_3 accounts for the major part of the atmospheric nitrate over the whole period of measurements, and we calculated an average proportion of 80 % of HNO_3 among total $f-NO_3^-$ (Davis et al., 2008, Fig. 3).

Over the 2009–2010 period, HNO_3 was measured at DC using annular denuder tube, with 48

155 sampling periods of 2.5 days on average (unpublished, personal communication, B. Jourdain and M. Legrand, 2012). These different sampling periods between the data sets hinder our ability to make a close comparison, but it is obvious that both times series show a very good agreement (data not shown). The ratio of HNO_3 to atmospheric nitrate is of the same order as that obtained at South Pole.

160 Another recent study presented a multi-year record of particulate nitrate at DC, collected on low volume sampler with Teflon filters (Traversi et al., 2014). Both the absolute nitrate concentration and the overall temporal pattern reported in that study are in good agreement with those of Erbland et al. (2013). By comparing the measurements of an 8-stage impactor along with those provided by a PM10 device, the authors concluded that during late summer (January and February), only 12.5 %

165 of atmospheric nitrate is collected on PM10 PTFE filters, while this fraction reaches 30 % for the November and December months. Thus, a more extensive characterisation of the temporal variation

in the partitioning between gaseous HNO_3 and particulate nitrate is needed to accurately retrieve HNO_3 concentration from atmospheric nitrate measurement.

To conclude, atmospheric nitrate measured at DC during several years using different methods shows a very consistent and reproducible temporal pattern. Further comparisons between gaseous and particulate fractions indicate that HNO_3 accounts for the major part of atmospheric nitrate. For sake of simplicity, we assume hereafter that the concentration of gaseous HNO_3 used as input in our model is equal to the concentration of atmospheric nitrate. This assumption will be further discussed along with the results of the model.

2.1.2 Snow nitrate

Nitrate concentration was measured year round between 2008 and 2010 during NITE DC program (NITrate Evolution in surface snow at Dome C). The skin layer (estimated average thickness of (4 ± 2) mm) was sampled once or twice a day during summer, and about once a week during winter (Erbland et al., 2013). The uncertainty ascribed to spatial variability and sampling method is estimated to be 20 %. In this study, we only used data from 30 January 2009 to 31 January 2010. This data set was already published (Erbland et al., 2013, Fig. 6), and is reproduced in Fig. 1a. NO_3^- concentration in the skin layer exhibits a seasonal pattern similar to that of atmospheric nitrate: it remains relatively low and steady during winter, with an average value of (161 ± 50) ng g^{-1} during the polar night, i.e. from March to September. Then, a sharp increase occurs around mid-November, with concentration in the 600–1400 ng g^{-1} range. The temporal lag of 3–4 weeks between the atmospheric and skin layer variations indicates a complex air–snow transfer function, that this work aims at elucidating by using a process-resolving model.

Further measurements of snow nitrate concentration were carried out in snow pits at DC, up to 50 cm deep every 6 weeks on average in winter (Fig. 2a), and up to 20 cm deep every week in summer (Fig. 2b). These concentration profiles of the upper snowpack give a better insight of the nitrogen recycling occurring in the snow. The highest concentration measured in summer is located in the top few mm to cm, whilst nitrate concentration dramatically decreases at greater depths, never exceeding 110 ng g^{-1} below 5 cm depth. During winter, the top 15–20 cm of the snowpack replenishes in nitrate, with concentration in the 200–400 ng g^{-1} range, whilst the deepest layer concentration decreases to less than 50 ng g^{-1}. This shows that nitrate undergoes an important seasonal recycling within the upper snowpack.

These temporal variations of NO_3^- observed in DC surface snow are also similar to the general trends featured by previous measurements in surface snow made at Halley station in coastal Antarctica from March 2004 to February 2005 (Wolff et al., 2008; Jones et al., 2011).

2.2 Snowpack physical properties

2.2.1 Snow temperature

Snow temperature is a key parameter for modelling snow chemistry since all processes implied in snow chemical exchange are temperature dependent. In addition, snow metamorphism and water vapour flux depend on temperature as well as on the vertical gradient of the temperature profile (see for instance Marbouty, 1980; Sommerfeld, 1983; Colbeck, 1989; Flin and Brzoska, 2008). We used modelled data to get snow surface temperature over the whole year of nitrate measurements.

A snowpack thermal diffusion model including a surface scheme coupled with a radiative transfer model to account precisely for the absorption of the radiation inside the snowpack is used. The snow-pack is discretised in horizontally homogeneous layers whose thickness increase exponentially with depth. The model takes as input meteorological forcing from ERA-Interim reanalysis and computes the evolution of temperature profile (Picard et al., 2009). Predictions were successfully compared to daily passive microwave satellite data, and a comparison with Brun et al. (2011) results shows good skills.

We used the modelled temperature in the uppermost 3 mm thick layer (which is also the surface "skin" temperature used in the surface energy budget calculation) and apply linear interpolation to down-scale the hourly data to 10 min, the timestep of our model. The modelled snow surface temperature is shown in Fig. 1b.

We compared the modelled temperature with skin temperature deduced from BSRN (baseline surface radiation network) upwelling longwave radiation observations (Christian Lanconelli, personal communication; see SI 1??). From this 3 month data set (from November 2009 to January 2010, raw data), the comparison revealed a small warm bias of the model (~ 2.5 K), and a slight underestimation of the amplitude of the diurnal cycle (see SI 1??) which agrees with other studies using ERA-Interim (Fréville et al., 2014). However, since this comparison was only possible during the summer, the same discrepancies between modelled and measured temperatures would not necessarily hold in winter.

2.2.2 Specific surface area

In our model, the physical description of the snow mainly relies on the snow specific surface area (SSA) value, which directly affects exchanges through the air–snow interface (see for example Dominé et al., 2008). Assuming spherical grains, the radius follows the relation:

$$R = \frac{3}{SSA \times \rho_{\text{ice}}} \tag{1}$$

where R is the radius (in m), SSA is the snow specific surface area (in $\mathrm{m^2\,kg^{-1}}$) and ρ_{ice} is the ice density, with $\rho_{\text{ice}} \simeq 924\,\mathrm{kg\,m^{-3}}$ (Hobbs, 1974, at -50 °C, DC annual mean temperature). When this study was initiated, the only SSA value reported at DC was 38.1 $\mathrm{m^2\,kg^{-1}}$ for the first centimetre,

decreasing monotonically to $13.6\ \mathrm{m^2\,kg^{-1}}$ at 70 cm depth (Gallet et al., 2011, Fig. 4 and Table A1).

235   Recent work specifically studying surface hoar at DC reported very close values, with an average of $39.0\ \mathrm{m^2\,kg^{-1}}$ for the top first centimetre of snow, and $26.4\ \mathrm{m^2\,kg^{-1}}$ for the second centimetre (Gallet et al., 2014). Thus, SSA was set to a value of $38.1\ \mathrm{m^2\,kg^{-1}}$ by default in the model, leading to a grain radius $R = 85\ \mu\mathrm{m}$. Recently Libois et al. (2015) investigated seasonal variations of SSA at DC showing that these values are typical of the summer while 2 to 3-fold higher values are observed

240   in winter. The effect of changing SSA was further tested in a sensitivity test presented in Sect. 5.4.

3   Model description

3.1   From gaseous HNO_3 to solid solution of nitrate in snow

A brief summary of the current knowledge about solvation steps which lead gaseous HNO_3 to form solid solution in bulk ice is presented in this section.

245   The uptake of trace gases on ice, and more specifically of acidic gases among which HNO_3, has been the subject of considerable investigation (see reviews by Abbatt, 2003; Huthwelker et al., 2006). Conceptually, this uptake proceeds firstly by molecular adsorption of HNO_3, followed by the ionisation (or dissociation) and then progressive solvation at the surface leading to a partial solvation shell (Buch et al., 2002; Bianco et al., 2007, 2008). In a second stage, thought to be much slower,

250   the adsorbed nitrate anions sink into the innermost crystal layers, leading to a complete solvation shell, and diffuse towards the bulk crystal. Recent studies addressed the ionisation state of HNO_3 adsorbed on ice surface, either using surface sensitive spectroscopy techniques (Křepelová et al., 2010; Marchand et al., 2012; Marcotte et al., 2013, 2015) or through molecular dynamics models (Riikonen et al., 2013, 2014). Molecular adsorbed state is found to be metastable, which happens

255   only at very low temperatures (45 K), whilst ionic dissociation occurs irreversibly upon heating at 120 K (Marchand et al., 2012). Molecular dynamics simulations suggest a pico and subpicosecond ionisation of HNO_3 in the defects sites (Riikonen et al., 2013), further supporting that molecular adsorption of HNO_3 on ice is a fleeting state prior to ionisation, at least for environmentaly relevant temperatures.

260   Despite these recent improvements in the understanding of HNO_3 ionisation following adsorption on an ice surface, the transition between surface (adsorption) and bulk (diffusion) processes still needs to be fully characterised. To the best of our knowledge, no process-scale parameterisation of the dissociation/solvation exists at the moment. Such parameterisation would be necessary to link surface and bulk concentrations, and further studies are thus needed to fully characterise the

265   transition between these states. For this reason, both processes were treated separately in our model. The model configuration 1 (adsorption) is described in the next section, while the configuration 2 (solid state diffusion) is described in Sect. 3.3.

3.2 Model configuration 1: adsorption

The HNO_3 surface coverage is a function of temperature and pressure only. Crowley et al. (2010) presented a compilation of data evaluated by a IUPAC subcommittee, that characterises heterogeneous processes on the surface of solid particles, including ice. They recommend the use of a single-site Langmuir isotherm which gives the fractional surface coverage θ:

$$\theta = \frac{N}{N_{\max}} = \frac{K_{\text{LangP}} \, P_{HNO_3}}{1 + K_{\text{LangP}} \, P_{HNO_3}} \tag{2}$$

where $N_{\max} = 2.7 \times 10^{18}$ molecules m^{-2} is the HNO_3 surface coverage at saturation,

$$K_{\text{LangP}} = \frac{K_{\text{LinC}} \, \mathcal{N}_A}{N_{\max} \, R \, T} \ (\text{in Pa}^{-1}) \tag{3}$$

$$K_{\text{LinC}} = 7.5 \times 10^{-7} \exp\left(\frac{4585}{T}\right) (\text{in m}) \tag{4}$$

K_{LangP} and K_{LinC} are partition coefficients expressed in different units, N is the HNO_3 surface coverage (in molecules m^{-2}), P_{HNO_3} is the HNO_3 partial pressure (in Pa), $\mathcal{N}_A$ is the Avogadro constant, T the snow temperature (in K) and R the molar gas constant ($R = 8.314$ J K^{-1} mol^{-1}).

This parameterisation is established for temperatures ranging from 214 K to 240 K, and is used here at DC temperatures, typically in the 200–250 K range. The conversion of surface coverage to bulk concentration is done using the SSA value:

$$[HNO_3] = \frac{N \times SSA}{\mathcal{N}_A} \tag{5}$$

where $[HNO_3]$ is the nitrate concentration (in mol m^{-3}).

The results and discussion following adsorption calculation are presented in Sect. 4.

3.3 Model configuration 2: solid state diffusion

In configuration 2, the model computes solid state diffusion in a layered snow grain. The outermost layer concentration or boundary condition (BC) was successively set according to three distinct parameterisations. Firstly, the NO_3^- concentration at the air – ice interface was set according to thermodynamic equilibrium (BC1). In a second stage, the kinetic, co-condensation process was taken into account through an empirical, diagnostic parameterisation (BC2), then with a physically based prognostic parameterisation (BC3). The general diffusion scheme and specific BCs are presented in the next sections.

3.3.1 Diffusion scheme

In configuration 2, the model considers a spherical snow grain with a radius $R = 85$ μm, divided in concentric layers of constant thickness $\delta r = 0.05$ μm. The model computes the solid state diffusion equation in spherical geometry with radial symmetry in the snow grain:

$$\frac{\partial C(r,t)}{\partial t} = D \left(\frac{2}{r} \frac{\partial C(r,t)}{\partial r} + \frac{\partial^2 C(r,t)}{\partial r^2} \right) \tag{6}$$

where $C(r,t)$ is nitrate concentration in the layer of radius r at time t, and D is the diffusion coefficient of HNO$_3$ in ice provided by Thibert and Dominé (1998):

$$D = 1.37 \times 10^{-4} \times 10^{-2610/T} \text{ (in m}^2\text{ s}^{-1}) \tag{7}$$

The modelled snow surface temperature ranges from 198 K to 253 K (average 222 K) during the studied period. The diffusion coefficient thus ranges from 8.9×10^{-18} m^2 s^{-1} to 6.4×10^{-15} m^2 s^{-1} (average 7.1×10^{-16} m^2 s^{-1}). A characteristic time for diffusion, τ, can be estimated as $\tau = l^2/D$ where l is a characteristic diffusion length. Considering the assumed spherical geometry of the snow grain, when diffusion reaches $0.21 \times R$, 50 % of the volume is affected; and when diffusion reaches $0.37 \times R$, 75 % of the volume is affected. Using these values as characteristic diffusion length and the average diffusion coefficient, the characteristic times for diffusion are $\tau_{.50} \simeq 5$ days and $\tau_{.75} \simeq 16$ days.

Thibert and Dominé (1998) indicated an uncertainty of ± 60 % for the diffusion coefficient, further explaining that it is probably the upper limit because of the existence of diffusion short pathways. The study by Thibert and Dominé (1998) was carried out at temperatures ranging from -8 °C to -35 °C. Nevertheless, Eq. (7) is applied to the temperature of DC surface snow, potentially leading to an increased uncertainty.

The concentration of the outermost layer of the modelled snow grain, which is the boundary condition (BC) of the diffusion equation (6), was successively parameterised in 3 different ways that are detailed in the next sections.

3.3.2 Equilibrium boundary condition (BC1)

In a first attempt labelled BC1, the outermost layer concentration was set according to the thermodynamic equilibrium solubility of HNO$_3$ in solid solution as measured by Thibert and Dominé (1998):

$$X^0_{\text{HNO}_3} = 2.37 \times 10^{-12} \exp\left(\frac{3532.2}{T}\right) P^{1/2.3}_{\text{HNO}_3} \tag{8}$$

where $X^0_{\text{HNO}_3}$ is the molar fraction of HNO$_3$ in ice, T is the snow temperature (in K) and P_{HNO_3} is the HNO$_3$ partial pressure (in Pa).

Thibert and Dominé (1998) indicated an uncertainty of ± 20 % for equilibrium solubility. The study by Thibert and Dominé (1998) was carried out at temperatures ranging from -8 °C to -35 °C. Nevertheless, as with the diffusion coefficient, Eq. (8) is also applied to the temperature of DC surface snow, potentially leading to an increased uncertainty.

The results and discussion of the modelling of nitrate concentration in surface snow using this BC1 approach are presented in Sect. 5.1. We also investigated how the uncertainties over the solubility and the diffusion coefficient affect the simulations, in a sensitivity study presented in Sect. 5.4.

3.3.3 Diagnostic co-condensation parameterisation (BC2)

To investigate the concentration of the growing phase, an empirical, diagnostic parameterisation of the co-condensation process was firstly developed. Valdez et al. (1989) carried out experiments on SO_2 incorporation into ice growing from water vapour, and reported that the amount of sulfur incorporated into the ice increased linearly with the amount of ice deposited. Jacob and Klockow (1993) compared the concentration of H_2O_2 in the gas phase and in the snow during fog events, and showed that the molar fraction of hydrogen peroxide, $X_{H_2O_2}$, resulting from co-condensation was similar to the ratio of partial pressures: $X_{H_2O_2} \simeq \frac{P_{H_2O_2}}{P_{H_2O}}$, as previously hypothesised by Sigg and Neftel (1988). Dominé et al. (1995) refined this analysis using the kinetics theory of gases to include the number of collisions, and further taking into account the surface accommodation coefficients α. They proposed that the molar fraction of a gas i (X_i) condensating along with water vapour should obey the following equation, where M is the molar mass:

$$X_i = \frac{P_i}{P_{H_2O}} \frac{\alpha_i}{\alpha_{H_2O}} \sqrt{\frac{M_{H_2O}}{M_i}} \tag{9}$$

However, Ullerstam and Abbatt (2005) carried out laboratory measurements of HNO_3 concentration in growing ice, and their results suggested that HNO_3 concentration was proportional to $P_{HNO_3}^{0.56}$ and independent of the water vapour partial pressure:

$$\log_{10}\left(X_{HNO_3}\right) = 0.56 \times \log_{10}\left(P_{HNO_3}\right) - 3.2 \tag{10}$$

where the exponent 0.56 could be explained by acid dissociation during co-condensation. Another possible explanation proposed by Ullerstam and Abbatt (2005) is that thermodynamic solubility governs at least partially the composition of a growing crystal as HNO_3 is sufficiently volatile and mobile to be excluded from the growing ice. Indeed, the power 0.56 dependence to HNO_3 partial pressure is close to that of thermodynamic equilibrium solubility (in Eq. (8), $1/2.3 \simeq 0.43$).

To summarise the conclusions of these studies, the co-condensed phase has a concentration which depends on (i) the studied trace gas partial pressure (but without agreement on the exponent in the case of HNO_3) and (ii) may or may not depend on the water vapour partial pressure. Thus, in order to test these hypotheses, a first simple diagnostic parameterisation of co-condensation process was implemented by adding an adjustable term to prescribe the outermost layer concentration (BC2):

$$X_{HNO_3} = X_{HNO_3}^0 + \alpha \cdot P_{HNO_3}^\beta \cdot P_{H_2O}^\gamma \tag{11}$$

where $X_{HNO_3}^0$ is the molar fraction of HNO_3 in ice given by thermodynamic equilibrium (see Eq. 8), P_{HNO_3} and P_{H_2O} are partial pressures of HNO_3 and water vapour, respectively (in Pa), and α, β, and γ are adjustable parameters. Solid state diffusion within the layered snow grain then proceeds as previously described (Sect. 3.3.1). The results of this BC2 configuration are presented in Sect. 5.2.

3.3.4 Prognostic co-condensation parameterisation (BC3)

365 In order to develop a physically based, prognostic parameterisation of the co-condensation process (BC3), the second step was to define the growth rate of snow crystals undergoing a temperature gradient. Calculation of the water vapour gradient inside the snowpack is a complex matter (Flin and Brzoska, 2008). Using upscaling theories, several recent studies aimed at obtaining macroscopic parameterisations ensued from an accurate description of the processes (heat conduction, vapour dif-

370 fusion, sublimation and condensation) occurring at the microscopic scale (Miller and Adams, 2009; Pinzer et al., 2012; Calonne et al., 2014; Hansen and Foslien, 2015). A major issue may arise when simply upscaling microscopic laws by using averaged, macroscopic parameters such as the temperature gradient. Indeed, as illustrated by Calonne et al. (2014, Fig. 4), microscale inhomogeneities are likely to enhance locally the temperature gradient, and thus the flux of water vapour. However,

375 Pinzer et al. (2012) compared the mass flux calculated using a macroscopic diffusion law on the one hand, and using two microscopic computations (particle image velocimetry and finite element simulation) on the other hand. They concluded that "the three methods of calculation coincide reasonably well", and thus that "the macroscopic vapour flux in snow can be calculated once the temperature gradient and the mean temperature of the snow are known, independently of the microstructure".

380 In the macroscopic diffusion law equation, Pinzer et al. (2012, Eq. (3)) used an effective diffusion coefficient for water vapour in the interstitial air, whose value has been a subject of debate for a long time (Calonne et al., 2014, and ref. therein). In their study, Calonne et al. (2014) concluded that the effective vapour diffusion is not enhanced in snow.

Based on these results, we assumed that a macroscopic scale water vapour flux can be reasonably

385 estimated using macroscopic, mean parameters. Following particulate growth laws in cloud models, Flanner and Zender (2006) proposed an equation giving the mass variation over time as a function of the water vapour gradient:

$$\frac{dm}{dt} = 4\pi R^2 D_v \left(\frac{d\rho_v}{dx}\right)_{x=R} \tag{12}$$

where R is the particle radius, D_v is the diffusivity of water vapour in air, and ρ_v is the water vapour

390 density (in $\mathrm{kg\,m^{-3}}$). The diffusivity of water vapour in air can be found in Pruppacher and Klett (1997) as a function of pressure and temperature, in the -40 °C to +40 °C range:

$$D_v = 2.11 \times 10^{-5} \left(\frac{T}{T_0}\right)^{1.94} \frac{P_0}{P} \ (\text{in } \mathrm{m^2\,s^{-1}}) \tag{13}$$

where $T_0 = 273.15$ K and $P_0 = 101325$ Pa. We stress here that the water vapour gradient in Eq. (12) was originally intended to be a microscopic gradient, but a macroscopic gradient derived from the

395 modelled temperature profile in the two uppermost layers was used. Because this growth law is used to parameterise the co-condensation process, only the cases leading to a mass increase were taken into account. Finally, the mass growth rate defined by Eq. (12) can be converted into a volume growth rate using ice density ρ_{ice}, and then to a radius growth Δr (in m) by assuming a uniform

condensation on the whole grain surface during a time Δt:

$$400 \quad \Delta r = \sqrt[3]{\frac{3}{4\pi}\left(\frac{1}{\rho_{\text{ice}}}4\pi R^2 D_v\left(\frac{\Delta\rho_v}{\Delta x}\right)_{x=R}\Delta t\right) + R^3} - R \quad\quad (14)$$

Note that in this equation Δr depends on $\Delta t^{1/3}$.

The last step of co-condensation parameterisation is to implement this dynamic feature of a growing crystal into the fixed shape of a spherical grain. An accurate modelling of temperature gradient metamorphism and ensuing co-condensation process would require a complex description of the
405 system, including snow grain shape, direction of growth, and local inhomogeneities, which is within the purview of snow microphysics 2-D or even 3-D state of the art models (see for example Flin et al., 2003; Kaempfer and Plapp, 2009; Calonne et al., 2014).

Another difficulty comes from the competition between co-condensation and diffusion. It was observed that the co-condensation process leads to out of thermodynamic equilibrium concentrations
410 (Bales et al., 1995; Dominé and Thibert, 1995, 1996; Ullerstam and Abbatt, 2005) that enhance solid state diffusion to re-equilibrate. The combination of these two processes was studied by Dominé and Thibert (1996) who proposed a theoretical description through a two-stage process. Firstly, a layer of thickness Δr and composition X_{kin} condensates at $t = 0$. Then, solid state diffusion takes place to re-equilibrate this layer towards the equilibrium concentration X_{eq}, until another layer condensates
415 at $t = \Delta t$, isolating the previous layer. According to this simplified description, the resulting molar fraction at a distance d from the surface and after a diffusion time t is given by:

$$X(d,t) = X_{\text{kin}} + (X_{\text{eq}} - X_{\text{kin}})\,\text{erfc}\left(\frac{d}{2\sqrt{D\,t}}\right) \quad\quad (15)$$

where X_{kin} is the molar fraction of the growing phase (which could be provided either by the gas kinetics theory parameterisation, Eq. (9), or by the empirical relation, Eq. (10)), X_{eq} is the molar
420 fraction inferred from thermodynamic equilibrium solubility (Eq. 8) and D is the diffusion coefficient of HNO_3 in ice (Eq. 7).

In Eq. (15), erfc is the complementary error function, with $\text{erfc}(0) = 1$ and $\text{erfc}(x)$ is decreasing towards zero for positive values. Since $\sqrt{D\,t}$ represents the typical diffusion length over a time t, the resulting molar fraction given by Eq. (15) will be close to X_{eq} if the condensed layer is thin
425 compared to the typical diffusion length, i.e. if the layer readily re-equilibrates through diffusion. On the contrary, if the condensed layer is thick, the resulting molar fraction gets closer to X_{kin}.

Following Dominé and Thibert (1996), the BC3 boundary condition defining the outermost layer concentration is set as $X(\Delta r, \Delta t)$ (Eq. 15) where Δr is the thickness of the condensed layer which has grown during the timestep Δt (Eq. 14). We emphasise that the radius of the modelled snow
430 grain is kept unchanged along the whole simulation. The calculation of the radius increase due to the condensation of water vapour is only used to compute the concentration (Eq. 15) at the surface of the modelled snow grain (BC).

4 Results and discussions for model configuration 1

The simulated nitrate concentration of the snow skin layer obtained in model configuration 1, involving only the adsorption process, is presented and discussed in this section.

4.1 Results

The evolution of the concentration of nitrate in the snow skin layer is plotted in Fig. 3. Undeniably, the adsorbed concentration modelled using non-dissociative Langmuir isotherms parameterisation does not fit with the measured concentration in three ways: firstly, the modelled concentration is higher than the measured ones during most of the year. From February to August, the average modelled concentration is 2.5-fold higher than the measured one, and this ratio increases to 8.3 from September to mid-November (see vertical separations in Fig. 3). On the contrary, the modelled concentration gradually decreases towards the end of January while the measured one reaches a seasonal maxima, leading to a ratio of 0.62 between modelled and measured concentrations during this last period. Secondly, the modelled concentration shows a strong diurnal variability following temperatures, with a ratio between daily maximum and minimum concentration regularly higher than 5, and with a yearly average equal to 2.6. By contrast, field measurements show weak diurnal variations of nitrate concentration in surface snow, and no anticorrelation with temperature (Fig. 2**??** in Supplement). The third major discrepancy is a premature seasonal maximum in the computation, starting late August and reaching maximum early November, while concentration measured in snow lags by 65 days.

The features of the modelled concentration attributed to adsorbed nitrate can be explained by the temperature and partial pressure dependencies of the adsorption isotherm. The surface coverage parameterisation strongly decreases with temperature (exponential function of the reciprocal temperature in Eq. (4)), whilst it increases roughly linearly with the HNO_3 partial pressure when the surface coverage is well below saturation. This explains the strong diurnal variations following the temperature cycle. It also explains the yearly pattern of the modelled concentration: firstly, during the winter, the very low temperature prevails over the low HNO_3 partial pressures, leading to modelled concentration already much higher than that measured. The influence of temperature is easily seen in April, May, and August, when temperature is the lowest (see Fig. 1b), leading to higher modelled concentration than in June and July, when temperature is higher and HNO_3 partial pressure is alike. Then, from early September to early November, HNO_3 partial pressure increases while temperature shows only a moderate increase, leading to the modelled peak of absorbed nitrate. Finally, nitrate partial pressure stays high until January, but this is counterbalanced by the temperature which increases to its yearly maximum, forcing modelled surface coverage to fall well under the measured values.

14

4.2 Discussion

Despite the use of the IUPAC current recommendation for the parameterisation of HNO_3 adsorption on ice, the modelled quantities adsorbed on snow are clearly incompatible with the measured concentration. In order to explain this discrepancy, we compared the experimental setups used in the various studies of adsorption (Abbatt, 1997; Arora et al., 1999; Hanson, 1992; Hudson et al., 2002; Hynes et al., 2002; Laird and Sommerfeld, 1995; Leu, 1988; Sokolov and Abbatt, 2002; Ullerstam et al., 2005; Zondlo et al., 1997). A review of these studies, and of the experimental techniques used, can be found in (Huthwelker et al., 2006). In brief, two main experimental techniques prevail: flow tubes, which were mostly used (Abbatt, 1997; Arora et al., 1999; Hanson, 1992; Hynes et al., 2002; Leu, 1988; Sokolov and Abbatt, 2002; Ullerstam et al., 2005), and Knudsen cells, which were used in two studies (Hudson et al., 2002; Zondlo et al., 1997). Whatever the technique used, ice was deposited on the reactor walls either by water vapour condensation (Hanson, 1992; Hudson et al., 2002; Leu, 1988; Zondlo et al., 1997), or by fast freezing an ice film (Abbatt, 1997; Hynes et al., 2002; Sokolov and Abbatt, 2002; Ullerstam et al., 2005).

A first pitfall which may arise from these studies comes from the lack of quantification of the exposed surface area of ice, which was measured only once by Hudson et al. (2002). They carried out several experiments at 209, 213 and 220 K, and found that the exposed surface was twice the geometrical surface. Leu et al. (1997) found that this ratio can be as high as ~ 9 in the case of ice formed by water vapour deposition at 196 K. These authors also reported that this ratio increases with the amount of water deposited, and also increases when the temperature decreases. On the other hand, in another study using ice formed by fast freezing a film of water, Abbatt et al. (2008) concluded that the ice was smooth at a molecular level, implying a ratio near 1. Yet, except in the study by Hudson et al. (2002), an under-estimation of the exposed surface, which leads to an overestimation of the surface coverage of ice, can not be ruled out.

All adsorption studies assumed that at very low temperatures, diffusion in bulk ice is negligible. However, even if the fraction of HNO_3 entering the bulk ice is small, neglecting it leads to a systematic overestimation of the surface coverage. Cox et al. (2005) analysed the data of Ullerstam et al. (2005) to include the diffusion process. Their study brought new insight about surface versus bulk processes, and their model performed well in reproducing adsorption curves when diffusion into the bulk was also taken into account. However, instead of using the existing parameterisation for nitrate solubility and diffusion coefficient in the ice (see Sect. 3.3.1 and 3.3.2), they made use of a simplified scheme to consider the diffusion process, which includes an adjustable rate coefficient for diffusion and hinders a close comparison with the above mentioned paramterisations. Furthermore, the desorption curves could not be well fitted by their model, especially for low surface coverage, indicating that the involved processes are still not fully understood and constrained.

The diffusion of nitrate into bulk ice could also have been further enhanced for three distinct reasons. Firstly, it is noteworthy that if the exposed surface area of ice is larger than the geometric

15

surface, this leads to a larger exchange interface, thus increasing the amount of HNO_3 diffusing to bulk ice in the total uptake. On the other hand, even if the ice covering the reactor's walls was smooth in the case of a frozen liquid film, the fast freezing process would very likely leads to a highly polycrystalline structure, where grain boundaries may act as shortcuts for the diffusion, thus enhancing bulk uptake. Last, several authors (Hudson et al., 2002; Hynes et al., 2002) pointed out that despite the careful attention to ensure that ice surface was in equilibrium with its vapour, part of the observed uptake could be ascribed to bulk incorporation of HNO_3 with condensing water if the exposed ice was slightly growing because of slight supersaturation or due to the highly dynamic air–ice interface (Bolton and Pettersson, 2000).

More generally, the question of the adsorbed state, closely linked to the ionisation process and to the reversibility of the adsorption, can also explain the mismatch between current parameterisation and measurements. In all the uptake experiments, it was observed that the total uptake splits between reversible and irreversible components, the former being only a minor part of the total. For instance, Ullerstam et al. (2005) reported that on average 20 % of the initial uptake was desorbing. Should a part of this irreversible uptake already account for a strongly bound, bulk uptake, that could explain a major part of the overestimation of the modelled absorbed concentration. New investigations are needed to gain a clearer view of the partitioning between surface and bulk.

Finally, several other uncertainties can be invoked to explain the discrepancies. The saturated surface coverages reported in the various studies range over almost one order of magnitude, from 1.2×10^{14} molec cm^2 (Arora et al., 1999) to 1.0×10^{15} molec cm^2 (Hynes et al., 2002). This uncertainty directly impacts the modelled surface coverage (Eq. 2). Secondly, most adsorption studies used HNO_3 partial pressure between 2 and 3 orders of magnitude higher than the one relevant at DC. Ullerstam et al. (2005) improved this, by using partial pressures down to $\sim 9 \times 10^{-7}$ Pa, however this remains ~ 25-times higher than the lowest partial pressures measured in winter at DC ($\sim 3.5 \times 10^{-8}$ Pa). Using their parameterisation in DC conditions thus implies a great extrapolation. The lack of data for very low partial pressures also enhances the uncertainties over the relevant type of adsorption isotherms, as the behaviour in the unsaturated region (i.e. at low partial pressure) provides more constraint over the best type of adsorption isotherms than that in (or near) the saturated region. This explains why several kinds of isotherms (dissociative (Hynes et al., 2002) or non-dissociative Langmuir isotherm (Ullerstam et al., 2005), Frenkel-Halsey-Hill isotherm (Hudson et al., 2002)) have been proposed, but no clear consensus has been achieved.

In order to test these different explanations, experimental setups should systematically include measurements of the exposed area of ice, and use partial pressures as low as possible. Processing the raw experimental data with the approach developed by Cox et al. (2005) seems a promising way to discriminate between surface and bulk uptake processes. Improvements of this approach could probably be achieved by using state-of-the-art parameterisation of the diffusion process.

540   Regarding the present study uncertainties, snow temperature and SSA and HNO_3 partial pressure
       are the three variables controlling the adsorbed surface coverage. HNO_3 partial pressure, assumed
       to be equal to the total atmospheric nitrate (see Sect. 2.1.1), is thus the upper limit. However, as pre-
       sented in the data description (see Sect. 2.1.1), this assumption likely leads to an overestimation no
       larger than 20 % on average, which cannot explain the overestimation of the modelled concentration
545   by a factor of 2.5–8.3. On the contrary, the warm bias of modelled temperatures (see Sect. 2.2.1 and
       SI 1**??**) leads to smaller modelled adsorption concentration, and the slightly reduced diurnal am-
       plitude tends to reduce this other discrepancy between modelled and measured concentration. Last,
       the SSA was kept constant during the whole simulation, but a recent study by Libois et al. (2015)
       indicated that the SSA value adopted in our model is comparable to summer observations, but is
550   2-3 lower than the winter SSA observations (see Sect. 2.2.2). At that time of the year, the modelled
       adsorbed concentration is already highly overestimated, thus accounting for a higher SSA would
       increase the discrepancy.

       To conclude this section, several reasons were invoked to explain the overestimation of the mod-
       elled adsorbed concentration. Given the inability of the current parameterisation to fit the measure-
555   ments and the major uncertainties related to the adsorption process, we decided thereafter to ignore
       the adsorbed concentration. In order to estimate the error thereby induced, we make the rough hy-
       pothesis that the current adsorption parameterisation is flawed by a constant overestimation factor.
       Decreasing the modelled adsorbed concentration by a constant factor of ~ 20 so that its envelope
       never exceeds measured concentration, leads to small adsorbed concentration during most of the
560   year excepted in early spring, i.e. in the September – early November peak period (see Fig. 3). In
       this situation, we estimate that adsorbed nitrate accounts for less than 13 % of snow nitrate on yearly
       average (less than 9 % when excluding the early September to early November period, and almost
       30 % during these 2 months), thus neglecting the adsorption process should lead to only minor er-
       ror, except during spring. One way to test this hypothesis is to carry out hourly measurements of
565   nitrate concentration in surface snow during spring. Owing to the strong temperature dependency of
       the adsorption isotherm, if adsorbed nitrate accounts for an important fraction of snow nitrate, then
       significant daily variations of snow nitrate concentrations should be observed.

5   Results and discussions for model configuration 2

       In this section, the model was run in configuration 2, based on the solid state diffusion process
570   (see Sect. 3.3). The results obtained with the three distinct BC parameterisations are successively
       presented and discussed hereafter.

5.1 Thermodynamic equilibrium concentration (BC1)

The first attempt to model nitrate concentration in the skin layer was done using solely the thermodynamic equilibrium concentration (see Sect. 3.3.2 and Eq. 8) to constrain the concentration of the external layer of the snow grain (BC1). The resulting concentration is plotted in Fig. 4 along with the measured concentration. The initial value of ~ 500 ng g^{-1} and the sharp decrease at the beginning of the serie (30/01/09 – 07/02/09) are due to the initialisation of the whole grain concentration to the closest measurement (point not shown, a few hours before the start of the simulation). The time needed to re-equilibrate the snow grain concentration, roughly 2 weeks, compares well with the characteristic diffusion time (see Sect. 3.3).

From mid-April to late October, the modelled concentration is in reasonable agreement with the measured concentration, with some features appearing to be reproduced by the model (a slight, steady increase lasting from July to August, followed by a trough and then a second slight increase period from September to mid-October). During this winter period, modelled concentration appears to be often slightly lower than measurements, and that point will be further discussed in the sensitivity study presented in Sect. 5.4. The modelled concentration also features smoother variations than the measured concentration, which can be mainly explained by the time resolution of HNO$_3$ partial pressure used as input, of roughly one week (see Sect. 2.1.1 and Fig. 1a). The good consistency between modelled and measured concentrations during winter months is an important result, as this indicates that winter concentration of nitrate in surface snow is mainly driven by the thermodynamic equilibrium solubility, coupled to solid state diffusion.

On the other hand, this first modelling attempt clearly fails to reproduce the summer peak of nitrate concentration in snow, with values in the 50-200 ng g^{-1} range from November to early April, while measured concentration peaks above 1400 ng g^{-1}. These results also show that summer concentration of nitrate in surface snow is highly enriched compared to what is expected from the thermodynamic equilibrium. These results demonstrate that another uptake process, driven by kinetics rather than thermodynamics, is needed to explain such high summer concentration.

5.2 Diagnostic co-condensation parameterisation (BC2)

The BC2 includes the kinetic co-condensation process, through the empirical diagnostic parameterisation presented in Sect. 3.3.3. We adjusted the 3 coefficients in Eq. (11) in order to minimise the RMSE between modelled and measured snow nitrate concentration. The optimal result, plotted in Fig. 6, was obtained with $X_{\text{HNO}_3} = X_{\text{HNO}_3}^0 + \alpha \cdot P_{\text{HNO}_3}^{0.43} \cdot P_{\text{H}_2\text{O}}^{1.27}$. The α parameter value was adjusted so that the amplitude of the modelled summer peak fit the data, but has no physical signification. However, the most relevant point to note is that the modelled peak is well in phase with the measurements (as a main difference with the adsorption), and both time series display similar features. Furthermore, it is noteworthy that including the co-condensation has not degraded the win-

18

ter prediction. Indeed, because of the very low winter temperature at DC, and given the exponential dependency of water vapour pressure over temperature, the co-condensation term becomes almost negligible (Town et al., 2008).

610   The optimum exponent for HNO_3 partial pressure is 0.43 which exactly corresponds to the exponent for HNO_3 partial pressure of thermodynamic equilibrium concentration (in Eq. (8), $1/2.3 \simeq 0.43$). Even if that needs to be confirmed by further investigations, this result tends to confirm the hypothesis formulated by Ullerstam and Abbatt (2005) that thermodynamic partitioning plays a role in the co-condensation process (see Sect. 3.3.3).

615   Because of the correct timing and shape of the modelled peak of nitrate, these results suggest that the co-condensation process is responsible of the out of equilibrium, high concentration of nitrate in the skin layer in summer. Among the two available laws giving X_{kin}, the concentration of the co-condensed phase (see Sect. 3.3.3 , Eq. (9) or (10)), the empirical one, whose dependency over the HNO_3 partial pressure is the closest to 0.43, seems the more suited to reproduce the observations.

620   **5.3   Prognostic co-condensation parameterisation (BC3)**

The last part of this work aimed at refining the parameterisation for the co-condensation process, using physically based variables. The prognostic parameterisation developed hereafter is refered as BC3. For sake of simplicity, and because the growth of snow grain is very slow compared to the recycling of vapor as suggested by Pinzer et al. (2012), a constant radius (R) is assumed. However,

625   the growth law defined in Eq. (12) is used in order to evaluate the equivalent radius increase Δr resulting from the co-condensation process during the model timestep Δt (Eq. 14). Finally, the concentration resulting from concomitant thermodynamic process (diffusion equilibration) and kinetic process (co-condensation process) is calculated using the theoretical Eq. (15) at a depth Δr, that is at the surface of the modelled snow grain whose radius is supposed to be constant.

630   The radius growth rate $\Delta r / \Delta t$ as derived from Eq. (14) is presented in Fig. 5. It spans roughly three orders of magnitude over the year, from about $10^{-12}\ \mathrm{m\,s^{-1}}$ in winter to $\sim 8 \times 10^{-10}\ \mathrm{m\,s^{-1}}$ in summer. The explanation of this behaviour is twofold. First, the diurnal temperature cycle has a larger amplitude in summer, which enhances the temperature gradient close to the surface. Second, the vapour pressure over ice increases exponentially with temperature. As a consequence, with a

635   given value of the temperature gradient, the gradient of water vapour concentration used in Eq. (12) is larger if temperatures are higher. This also explains the diurnal variation of the grain radius growth. The most striking feature of the radius growth rate is that it peaks during the same period of the year that the peak of nitrate concentration in the skin layer. The yearly pattern of the radius growth rate predicted by our model is also consistent with independent studies focused on snow physical

640   properties (Picard et al., 2012; Libois et al., 2015). This comes as another evidence that snow metamorphism, and co-condensation, have a major influence over the snow chemical concentration.

19

The resulting modelled nitrate concentration in surface snow is presented in Fig. 6. In Table 1, a summary of the model runs, along with their RMSE, is presented . Simulation results are similar to those obtained with the BC2 parameterisation, but with a slightly improved RMSE. A diurnal variation of the modelled concentration is observed, as a consequence of the diurnal variation of the radius growth rate. However, the diurnal variation of the concentration is much smoother because solid state diffusion in the whole snow grain softens the large diurnal variations in the outermost layer of the snow grain. The relative diurnal variation of the concentration is smaller than 20 %, which is similar to the measurements uncertainty due to spatial heterogeneity. In this physically based parameterisation, a slight dependency of the results to the model timestep arises. This is explained by the radius increase Δr which depends on the cubic root of the time (Eq. 14), and which is divided by the square root of the time in Eq. (15). To compensate this dependency, either the timestep of the model needs to be adjusted for optimum results, or an additional correction factor can be used in order to keep the timestep unchanged, with a value well suited regarding the diffusion process. The exact reason of this dependency over the time step is complex to establish, but can very likely be ascribed to the hypothesised geometry of the snow grain (a sphere) and of the condensed phase (a layer). Improving this point necessitates determination of the relationship between mean thickness of the co-condensed layer as a function of time.

In Fig. 6, the modelled concentration shows a poorer fit with the measured concentration during spring, just before the observed peak of snow nitrate. This is confirmed by a monthly regression analysis (see Table SI 1**??**) which shows a lower correlation from September to November, which corresponds to the period where the modelled adsorption peaks (see Fig. 3). This is another indication that adsorbed nitrate may account for a noticeable part of surface snow nitrate in early spring.

The photolysis has not been included in this study, because the dramatic increase of summer nitrate concentration in the skin layer demonstrate that uptake processes overtake loss processes in this specific layer. In order to refine this comparison regarding the budget of nitrate in the skin layer, an estimation of the uptake and destruction fluxes is presented in the Supplementary Information (Sect. 3**??**). It appears that the uptake flux calculated with the BC3 parameterisation is 1.5 orders of magnitude larger than the loss flux due to photolysis. This confirms that photolysis loss is negligible as compared to the co-condensation uptake when studying the skin layer concentration.

Given the numerous assumptions made in the model, the overall reproduction of the measurements by the parameterisation including co-condensation appears satisfactory.

5.4 Sensitivity study

In order to further investigate the modelling uncertainties, the sensitivity of the model to the thermodynamic equilibrium concentration, diffusion coefficient and SSA value is evaluated. A synthesis of RMSE values of the sensitivity runs is presented in Table 1.

As shown in Sect. 5.1, winter modelled concentration underestimates the measurements, which could be explained by an underestimated thermodynamic equilibrium solubility (Eq. 8). The best fit with the data is obtained for an increase of 39 % (see Table 1). This optimum increase is almost twice as much as the uncertainty reported by Thibert and Dominé (1998, 20 %), however we applied the solubility parameterisation at much lower temperature than in their study.

A few measurements of the ratio of HNO_3 over atmospheric nitrate presented in Sect. 2.1.1 suggest that HNO_3 might account for roughly 70–90 % of atmospheric nitrate. Taking this ratio into account would reduce the HNO_3 partial pressure used as input in the model, but might be counterbalanced by a further increase of the thermodynamic solubility. New studies are needed to confirm the speciation of atmospheric nitrate and its seasonal variation. On the other hand, the current underestimation of the modelled concentration during winter can also be partly ascribed to a small adsorbed fraction amongst the total snow nitrate.

Secondly, using a diffusion coefficient lower than that suggested by Thibert and Dominé (1998, Eq. 7) generally improves the simulation performance. Using BC3 simulation as a reference, decreasing the diffusion coefficient by 72 % leads to the best reproduction of the results (see Table 1). When the solubility value increased by 39 % is used, the diffusion coefficient is decreased by 64 %. Thibert and Dominé (1998) reported a 60 % uncertainty for the diffusion coefficient, and indicated that their parameterisation likely represents the upper bounds, which compares well with the sensitivity analysis result.

However, another explanation is possible, because a decrease of the SSA has a similar effect to a decrease of the diffusion coefficient, as they both slow down the diffusion. Decreasing the SSA to $23 \mathrm{~m}^2 \mathrm{~kg}^{-1}$ leads to almost the same result as a decrease of 64 % of the diffusion coefficient (see Table 1). In the current version of the model, the radius of the snow grain is kept constant over time as a simple hypothesis, but it has been shown by Picard et al. (2012); Libois et al. (2015) that snow grain size features a sharp increase at DC during December and January, when the modelled water vapour fluxes driving the co-condensation process are highest. It is remarkable that the optimum value of $23 \mathrm{~m}^2 \mathrm{~kg}^{-1}$ is in very good agreement with that observed in summer Libois et al. (2015, Fig. 1). Future development of the current work should consider grain size change to distinguish between these two alternative hypotheses.

6 Conclusions

In this study we investigated the role of three processes that intervene in air–snow exchange of nitrate at DC. It revealed that the co-condensation of nitrate along with the condensation of water vapour flux driven by thermal gradient metamorphism is a major process, absolutely needed to explain the summer peak of nitrate measured in surface snow.

This study further reveals that the current state-of-the-art parameterisation for HNO_3 adsorption on snow leads to modelled concentration which differs from the observations, and cannot be used without major changes. We propose the hypothesis that adsorption measurements of HNO_3 on ice attributed most, if not all, of the uptake to the only adsorption process, while a noticeable part of this uptake should in fact be ascribed to bulk, irreversible incorporation. New laboratory investigations should be conducted along with theoretical studies in order to improve the current understanding of the binding process occurring on the ice surface and its kinetics, in order to make a clearer distinction between surface and bulk nitrate on the ice. On the contrary, studies aiming at the determination of equilibrium solubility and diffusion coefficient of nitrate in the ice take advantage of "integrative" measurements, in the sense that these two properties are deduced from macroscopic concentration profiles in the ice, without needing further hypothesis or insight about the actual microscopic processes occurring at the air–ice interface (binding, ionisation, solvation). This different approach probably explains why, despite being much less numerous, these studies provided robust parameterisations. Assuming that the adsorption parameterisation is overestimated by a constant factor which would leave the yearly pattern unchanged, the maximum featured by the modelled adsorbed concentration in September and October suggests that adsorbed nitrate might account for roughly 30 % of snow nitrate during these 2 months. As for the rest of the year and based on the same hypothesis, adsorbed nitrate should account for less than 10 % of snow nitrate.

Thus, by ignoring the adsorption process, and focusing solely on the solid state diffusion inside a spherical snow grain, we developed a physically based parameterisation for the concentration at the surface of this grain, used as the boundary condition of the diffusion equation. This parameterisation includes both thermodynamic equilibrium concentration and co-condensation process. Without needing any further adjustment parameter, the implementation of this newly developed parameterisation allowed a satisfactory reproduction of the one-year long dataset of nitrate concentration in DC surface snow. Given the similar general features of the measurements of atmospheric and snow nitrate in other Antarctica sites such as South Pole or even Halley, it seems very likely that the overall modelling framework that we developed can generalise at least over the Antarctic plateau.

Even if some improvements still need to be done, especially regarding a more realistic geometry of the co-condensed phase, the developed parameterisation and the overall modelling scheme can already be implemented as a foundation piece in one-dimensional (1-D) snow–atmosphere models. Some new insights over nitrogen recycling inside the snowpack could ensue from such vertical, 1-D modelling. In this study focused on skin layer snow, nitrate photolysis inside the snow grain has not been implemented since nitrate loss is much weaker than uptake for this specific layer, as demonstrated by the dramatic increase of nitrate concentration during summer. This is not true for the whole snowpack, and photolysis should be included in a 1-D snow chemistry model. For that purpose, the description of a snow grain as a layered medium will enable using of different quantum

yields, after some studies suggested that it span more than 2 orders of magnitude depending on the availability of nitrate inside the ice matrix (Zhu et al., 2010; Meusinger et al., 2014).

Ultimately, this work shows that snow physics and snow chemistry are tightly coupled, and especially that snow metamorphism resulting mainly from temperature gradients does not affect solely the physical properties of the snow, but also its chemical composition. It is also noteworthy that physical exchange processes on their own appear to explain a major part of the observed changes in surface snow nitrate at DC. Thus, it seems highly necessary that any field campaign mainly dedicated to snow chemistry also devote efforts to precise measurements of snow physical properties.

References

Abbatt, J. P. D.: Interaction of HNO_3 with water–ice surfaces at temperatures of the free troposphere, Geophysical Research Letters, 24, 1479–1482, doi:10.1029/97GL01403, 1997.

Abbatt, J. P. D.: Interactions of atmospheric trace gases with ice surfaces: adsorption and reaction, Chemical Reviews, 103, 4783–4800, doi:10.1021/cr0206418, 2003.

Abbatt, J. P. D., Bartels-Rausch, T., Ullerstam, M., and Ye, T. J.: Uptake of acetone, ethanol and benzene to snow and ice: effects of surface area and temperature, Environmental Research Letters, 3, 045 008, doi:10.1088/1748-9326/3/4/045008, 2008.

Arimoto, R., Zeng, T., Davis, D., Wang, Y., Khaing, H., Nesbit, C., and Huey, G.: Concentrations and sources of aerosol ions and trace elements during ANTCI-2003, Atmospheric Environment, 42, 2864–2876, doi:10.1016/j.atmosenv.2007.05.054, 2008.

Arora, O. P., Cziczo, D. J., Morgan, A. M., Abbatt, J. P. D., and Niedziela, R. F.: Uptake of nitric acid by sub-micron-sized ice particles, Geophysical Research Letters, 26, 3621–3624, doi:10.1029/1999GL010881, 1999.

Bales, R. C., Losleben, M. V., McConnell, J. R., Fuhrer, K., and Neftel, A.: H_2O_2 in snow, air and open pore space in firn at Summit, Greenland, Geophysical Research Letters, 22, 1261–1264, doi:10.1029/95GL01110, 1995.

Barret, M., Dominé, F., Houdier, S., Gallet, J.-C., Weibring, P., Walega, J., Fried, A., and Richter, D.: Formaldehyde in the Alaskan Arctic snowpack: partitioning and physical processes involved in air-snow exchanges, Journal of Geophysical Research, 116, D00R03, doi:10.1029/2011JD016038, 2011a.

Barret, M., Houdier, S., and Dominé, F.: Thermodynamics of the formaldehyde–water and formaldehyde–ice systems for atmospheric applications, The Journal of Physical Chemistry A, 115, 307–317, doi:10.1021/jp108907u, 2011b.

Beine, H., Dominé, F., Simpson, W., Honrath, R., Sparapani, R., Zhou, X., and King, M.: Snow-pile and chamber experiments during the Polar Sunrise Experiment 'Alert 2000': exploration of nitrogen chemistry, Atmospheric Environment, 36, 2707–2719, doi:10.1016/S1352-2310(02)00120-6, 2002.

Berhanu, T. A., Meusinger, C., Erbland, J., Jost, R., Bhattacharya, S. K., Johnson, M. S., and Savarino, J.: Laboratory study of nitrate photolysis in Antarctic snow. II. Isotopic effects and wavelength dependence, The Journal of Chemical Physics, 140, 244 306, doi:10.1063/1.4882899, 2014.

Bianco, R., Wang, S., and Hynes, J. T.: Theoretical study of the dissociation of nitric acid at a model aqueous surface, The Journal of Physical Chemistry A, 111, 11 033–11 042, doi:10.1021/jp075054a, 2007.

Bianco, R., Wang, S., and Hynes, J. T.: Infrared signatures of HNO_3 and NO_3^- at a model aqueous surface. A theoretical study, The Journal of Physical Chemistry A, 112, 9467–9476, doi:10.1021/jp802563g, 2008.

Bock, J. and Jacobi, H.-W.: Development of a mechanism for nitrate photochemistry in snow, The Journal of Physical Chemistry A, 114, 1790–1796, doi:10.1021/jp909205e, 2010.

Bolton, K. and Pettersson, J. B. C.: A molecular dynamics study of the long-time ice Ih surface dynamics, The Journal of Physical Chemistry B, 104, 1590–1595, doi:10.1021/jp9934883, 2000.

Boxe, C. S. and Saiz-Lopez, A.: Multiphase modeling of nitrate photochemistry in the quasi-liquid layer (QLL): implications for NO_x release from the Arctic and coastal Antarctic snowpack, Atmospheric Chemistry and Physics, 8, 4855–4864, doi:10.5194/acp-8-4855-2008, 2008.

Brun, E., Six, D., Picard, G., Vionnet, V., Arnaud, L., Bazile, E., Boone, A., Bouchard, A., Genthon, C., Guidard, V., Le Moigne, P., Rabier, F., and Seity, Y.: Snow/atmosphere coupled simulation at Dome C, Antarctica, Journal of Glaciology, 57, 721–736, doi:10.3189/002214311797409794, 2011.

Buch, V., Sadlej, J., Aytemiz-Uras, N., and Devlin, J. P.: Solvation and ionization stages of HCl on ice nanocrystals, The Journal of Physical Chemistry A, 106, 9374–9389, doi:10.1021/jp021539h, 2002.

Calonne, N., Geindreau, C., and Flin, F.: Macroscopic modeling for heat and water vapor transfer in dry snow by homogenization, The Journal of Physical Chemistry B, 118, 13 393–13 403, doi:10.1021/jp5052535, 2014.

Champollion, N., Picard, G., Arnaud, L., Lefebvre, E., and Fily, M.: Hoar crystal development and disappearance at Dome C, Antarctica: observation by near-infrared photography and passive microwave satellite, The Cryosphere, 7, 1247–1262, doi:10.5194/tc-7-1247-2013, 2013.

Chu, L. and Anastasio, C.: Quantum yields of hydroxyl radical and nitrogen dioxide from the photolysis of nitrate on ice, The Journal of Physical Chemistry A, 107, 9594–9602, doi:10.1021/jp0349132, 2003.

Chu, L. and Anastasio, C.: Temperature and wavelength dependence of nitrite photolysis in frozen and aqueous solutions, Environmental Science & Technology, 41, 3626–3632, doi:10.1021/es062731q, 2007.

Clapsaddle, C. and Lamb, D.: The sorption behavior of SO_2 on ice at temperatures between -30 °C and -5 °C, Geophysical Research Letters, 16, 1173–1176, doi:10.1029/GL016i010p01173, 1989.

Colbeck, S.: Snow-crystal growth with varying surface temperatures and radiation penetration, Journal of Glaciology, 35, 23–29, doi:10.3189/002214389793701536, 1989.

Conklin, M. H. and Bales, R. C.: SO_2 uptake on ice spheres: liquid nature of the ice-air interface, Journal of Geophysical Research, 98, 16 851–16 855, doi:10.1029/93JD01207, 1993.

Conklin, M. H., Sigg, A., Neftel, A., and Bales, R. C.: Atmosphere-snow transfer function for H_2O_2: microphysical considerations, Journal of Geophysical Research, 98, 18 367–18 376, doi:10.1029/93JD01194, 1993.

Cotter, E. S. N., Jones, A. E., Wolff, E. W., and Bauguitte, S. J.-B.: What controls photochemical NO and NO_2 production from Antarctic snow? Laboratory investigation assessing the wavelength and temperature dependence, Journal of Geophysical Research, 108, 4147, doi:10.1029/2002JD002602, 2003.

Cox, R. A., Fernandez, M. A., Symington, A., Ullerstam, M., and Abbatt, J. P. D.: A kinetic model for uptake of HNO_3 and HCl on ice in a coated wall flow system, Physical Chemistry Chemical Physics, 7, 3434–3442, doi:10.1039/b506683b, 2005.

Crowley, J. N., Ammann, M., Cox, R. A., Hynes, R. G., Jenkin, M. E., Mellouki, A., Rossi, M. J., Troe, J., and Wallington, T. J.: Evaluated kinetic and photochemical data for atmospheric chemistry: Volume V – heterogeneous reactions on solid substrates, Atmospheric Chemistry and Physics, 10, 9059–9223, doi:10.5194/acp-10-9059-2010, 2010.

Davis, D., Eisele, F., Chen, G., Crawford, J., Huey, G., Tanner, D., Slusher, D., Mauldin, L., Oncley, S., Lenschow, D., Semmer, S., Shetter, R., Lefer, B., Arimoto, R., Hogan, A., Grube, P., Lazzara, M., Bandy, A., Thornton, D., Berresheim, H., Bingemer, H., Hutterli, M., McConnell, J., Bales, R., Dibb, J., Buhr, M., Park, J., McMurry, P., Swanson, A., Meinardi, S., and Blake, D.: An overview of ISCAT 2000, Atmospheric Environment, 38, 5363–5373, doi:10.1016/j.atmosenv.2004.05.037, 2004.

Davis, D., Seelig, J., Huey, G., Crawford, J., Chen, G., Wang, Y., Buhr, M., Helmig, D., Neff, W., and Blake, D.: A reassessment of Antarctic plateau reactive nitrogen based on ANTCI 2003 airborne and ground based measurements, Atmospheric Environment, 42, 2831–2848, doi:10.1016/j.atmosenv.2007.07.039, 2008.

Dibb, J. E., Talbot, R. W., Munger, J. W., Jacob, D. J., and Fan, S.-M.: Air-snow exchange of HNO_3 and NO_y at Summit, Greenland, Journal of Geophysical Research, 103, 3475–3486, doi:10.1029/97JD03132, 1998.

Dibb, J. E., Arsenault, M., Peterson, M. C., and Honrath, R. E.: Fast nitrogen oxide photochemistry in Summit, Greenland snow, Atmospheric Environment, 36, 2501–2511, doi:10.1016/S1352-2310(02)00130-9, 2002.

Dominé, F. and Rauzy, C.: Influence of the ice growth rate on the incorporation of gaseous HCl, Atmospheric Chemistry and Physics, 4, 2513–2519, doi:10.5194/acp-4-2513-2004, 2004.

Dominé, F. and Thibert, E.: Relationship between atmospheric composition and snow composition for HCl and HNO_3, in: Proceedings of a Boulder Symposium, IAHS Publ. n° 228, pp. 3–10, Kathy A. Tonnessen, Mark W. Williams and Martyn Tranter, Boulder, Colorado, 1995.

Dominé, F. and Thibert, E.: Mechanism of incorporation of trace gases in ice grown from the gas phase, Geophysical Research Letters, 23, 3627–3630, doi:10.1029/96GL03290, 1996.

Dominé, F., Thibert, E., Van Landeghem, F., Silvente, E., and Wagnon, P.: Diffusion and solubility of HCl in ice: preliminary results, Geophysical Research Letters, 21, 601–604, doi:10.1029/94GL00512, 1994.

Dominé, F., Albert, M., Huthwelker, T., Jacobi, H. W., Kokhanovsky, A. A., Lehning, M., Picard, G., and Simpson, W. R.: Snow physics as relevant to snow photochemistry, Atmospheric Chemistry and Physics, 8, 171–208, doi:10.5194/acp-8-171-2008, 2008.

Dominé, F., Bock, J., Voisin, D., and Donaldson, D. J.: Can we model snow photochemistry? Problems with the current approaches, The Journal of Physical Chemistry A, 117, 4733–4749, doi:10.1021/jp3123314, 2013.

Dominé, F., Thibert, E., Silvente, E., Legrand, M., and Jaffrezo, J.-L.: Determining past atmospheric HCl mixing ratios from ice core analyses, Journal of Atmospheric Chemistry, 21, 165–186, doi:10.1007/BF00696579, 1995.

Dubowski, Y., Colussi, A. J., and Hoffmann, M. R.: Nitrogen dioxide release in the 302 nm band photolysis of spray-frozen aqueous nitrate solutions. Atmospheric implications, The Journal of Physical Chemistry A, 105, 4928–4932, doi:10.1021/jp0042009, 2001.

Dubowski, Y., Colussi, A. J., Boxe, C., and Hoffmann, M. R.: Monotonic increase of nitrite yields in the photolysis of nitrate in ice and water between 238 and 294 K, The Journal of Physical Chemistry A, 106, 6967–6971, doi:10.1021/jp0142942, 2002.

Ebner, P. P., Andreoli, C., Schneebeli, M., and Steinfeld, A.: Tomography-based characterization of ice-air interface dynamics of temperature gradient snow metamorphism under advective conditions: TEMPERATURE GRADIENT SNOW METAMORPHISM, Journal of Geophysical Research: Earth Surface, 120, 2437–2451, doi:10.1002/2015JF003648, 2015.

Eisele, F., Davis, D., Helmig, D., Oltmans, S., Neff, W., Huey, G., Tanner, D., Chen, G., Crawford, J., and Arimoto, R.: Antarctic Tropospheric Chemistry Investigation (ANTCI) 2003 overview, Atmospheric Environment, 42, 2749–2761, doi:10.1016/j.atmosenv.2007.04.013, 2008.

Erbland, J., Vicars, W. C., Savarino, J., Morin, S., Frey, M. M., Frosini, D., Vince, E., and Martins, J. M. F.: Air–snow transfer of nitrate on the East Antarctic Plateau – Part 1: isotopic evidence for a photolytically driven

dynamic equilibrium in summer, Atmospheric Chemistry and Physics, 13, 6403–6419, doi:10.5194/acp-13-6403-2013, 2013.

885   Erbland, J., Savarino, J., Morin, S., France, J. L., Frey, M. M., and King, M. D.: Air–snow transfer of nitrate on the East Antarctic Plateau – Part 2: An isotopic model for the interpretation of deep ice-core records, Atmospheric Chemistry and Physics, 15, 12 079–12 113, doi:10.5194/acp-15-12079-2015, 2015.

Finlayson-Pitts, B. J. and Pitts, J. N.: Chemistry of the upper and lower atmosphere: theory, experiments, and applications, Academic Press, San Diego, 2000.

890   Flanner, M. G. and Zender, C. S.: Linking snowpack microphysics and albedo evolution, Journal of Geophysical Research, 111, D12 208, doi:10.1029/2005JD006834, 2006.

Flin, F. and Brzoska, J.-B.: The temperature-gradient metamorphism of snow: vapour diffusion model and application to tomographic images, Annals of Glaciology, 49, 17–21, doi:10.3189/172756408787814834, 2008.

895   Flin, F., Brzoska, J.-B., Lesaffre, B., Coléou, C., and Pieritz, R. A.: Full three-dimensional modelling of curvature-dependent snow metamorphism: first results and comparison with experimental tomographic data, Journal of Physics D: Applied Physics, 36, A49–A54, doi:10.1088/0022-3727/36/10A/310, 2003.

Frey, M. M., Savarino, J., Morin, S., Erbland, J., and Martins, J. M. F.: Photolysis imprint in the nitrate stable isotope signal in snow and atmosphere of East Antarctica and implications for reactive nitrogen cycling,

900   Atmospheric Chemistry and Physics, 9, 8681–8696, doi:10.5194/acp-9-8681-2009, 2009.

Fréville, H., Brun, E., Picard, G., Tatarinova, N., Arnaud, L., Lanconelli, C., Reijmer, C., and van den Broeke, M.: Using MODIS land surface temperatures and the Crocus snow model to understand the warm bias of ERA-Interim reanalyses at the surface in Antarctica, The Cryosphere, 8, 1361–1373, doi:10.5194/tc-8-1361-2014, 2014.

905   Gallet, J.-C., Dominé, F., Arnaud, L., Picard, G., and Savarino, J.: Vertical profile of the specific surface area and density of the snow at Dome C and on a transect to Dumont D'Urville, Antarctica – albedo calculations and comparison to remote sensing products, The Cryosphere, 5, 631–649, doi:10.5194/tc-5-631-2011, 2011.

Gallet, J.-C., Dominé, F., Savarino, J., Dumont, M., and Brun, E.: The growth of sublimation crystals and surface hoar on the Antarctic plateau, The Cryosphere, 8, 1205–1215, doi:10.5194/tc-8-1205-2014, 2014.

910   Hansen, A. C. and Foslien, W. E.: A macroscale mixture theory analysis of deposition and sublimation rates during heat and mass transfer in dry snow, The Cryosphere, 9, 1857–1878, doi:10.5194/tc-9-1857-2015, 2015.

Hanson, D. R.: The uptake of HNO_3 onto ice, NAT, and frozen sulfuric acid, Geophysical Research Letters, 19, 2063–2066, doi:10.1029/92GL02182, 1992.

915   Hobbs, P. V.: Ice physics, Clarendon Press, Oxford, 1974.

Honrath, R., Lu, Y., Peterson, M., Dibb, J., Arsenault, M., Cullen, N., and Steffen, K.: Vertical fluxes of NO_x, HONO, and HNO_3 above the snowpack at Summit, Greenland, Atmospheric Environment, 36, 2629–2640, doi:10.1016/S1352-2310(02)00132-2, 2002.

Honrath, R. E., Peterson, M. C., Guo, S., Dibb, J. E., Shepson, P. B., and Campbell, B.: Evidence of NO_x

920   production within or upon ice particles in the Greenland snowpack, Geophysical Research Letters, 26, 695–698, doi:10.1029/1999GL900077, 1999.

Honrath, R. E., Guo, S., Peterson, M. C., Dziobak, M. P., Dibb, J. E., and Arsenault, M. A.: Photochemical production of gas phase NO_x from ice crystal NO_3^-, Journal of Geophysical Research, 105, 24 183–24 190, doi:10.1029/2000JD900361, 2000a.

925 Honrath, R. E., Peterson, M. C., Dziobak, M. P., Dibb, J. E., Arsenault, M. A., and Green, S. A.: Release of NO_x from sunlight-irradiated midlatitude snow, Geophysical Research Letters, 27, 2237–2240, doi:10.1029/1999GL011286, 2000b.

Hudson, P. K., Shilling, J. E., Tolbert, M. A., and Toon, O. B.: Uptake of nitric acid on ice at tropospheric temperatures: implications for cirrus clouds, The Journal of Physical Chemistry A, 106, 9874–9882, 930 doi:10.1021/jp020508j, 2002.

Huthwelker, T., Lamb, D., Baker, M., Swanson, B., and Peter, T.: Uptake of SO_2 by polycrystalline water ice, Journal of Colloid and Interface Science, 238, 147–159, doi:10.1006/jcis.2001.7507, 2001.

Huthwelker, T., Ammann, M., and Peter, T.: The uptake of acidic gases on ice, Chemical Reviews, 106, 1375–1444, doi:10.1021/cr020506v, 2006.

935 Hutterli, M. A., Röthlisberger, R., and Bales, R. C.: Atmosphere-to-snow-to-firn transfer studies of HCHO at Summit, Greenland, Geophysical Research Letters, 26, 1691–1694, doi:10.1029/1999GL900327, 1999.

Hutterli, M. A., Bales, R. C., McConnell, J. R., and Stewart, R. W.: HCHO in Antarctic snow: preservation in ice cores and air-snow exchange, Geophysical Research Letters, 29, 1235, doi:10.1029/2001GL014256, 2002.

940 Hutterli, M. A., McConnell, J. R., Bales, R. C., and Stewart, R. W.: Sensitivity of hydrogen peroxide (H_2O_2) and formaldehyde (HCHO) preservation in snow to changing environmental conditions: implications for ice core records, Journal of Geophysical Research, 108, 4023, doi:10.1029/2002JD002528, 2003.

Hynes, R. G., Fernandez, M. A., and Cox, R. A.: Uptake of HNO_3 on water-ice and coadsorption of HNO_3 and HCl in the temperature range 210–235 K, Journal of Geophysical Research, 107, 4797, 945 doi:10.1029/2001JD001557, 2002.

Jacob, P. and Klockow, D.: Measurements of hydrogen peroxide in Antarctic ambient air, snow and firn cores, Fresenius' Journal of Analytical Chemistry, 346, 429–434, doi:10.1007/BF00325856, 1993.

Jacobi, H.-W. and Hilker, B.: A mechanism for the photochemical transformation of nitrate in snow, Journal of Photochemistry and Photobiology A: Chemistry, 185, 371–382, doi:10.1016/j.jphotochem.2006.06.039, 950 2007.

Jones, A. E., Weller, R., Wolff, E. W., and Jacobi, H. W.: Speciation and rate of photochemical NO and NO_2 production in Antarctic snow, Geophysical Research Letters, 27, 345–348, doi:10.1029/1999GL010885, 2000.

Jones, A. E., Wolff, E. W., Salmon, R. A., Bauguitte, S. J.-B., Roscoe, H. K., Anderson, P. S., Ames, D., Clemitshaw, K. C., Fleming, Z. L., Bloss, W. J., Heard, D. E., Lee, J. D., Read, K. A., Hamer, P., Shallcross, 955 D. E., Jackson, A. V., Walker, S. L., Lewis, A. C., Mills, G. P., Plane, J. M. C., Saiz-Lopez, A., Sturges, W. T., and Worton, D. R.: Chemistry of the Antarctic boundary layer and the interface with snow: an overview of the CHABLIS campaign, Atmospheric Chemistry and Physics, 8, 3789–3803, doi:10.5194/acp-8-3789-2008, 2008.

Jones, A. E., Wolff, E. W., Ames, D., Bauguitte, S. J.-B., Clemitshaw, K. C., Fleming, Z., Mills, G. P., Saiz-960 Lopez, A., Salmon, R. A., Sturges, W. T., and Worton, D. R.: The multi-seasonal NO_y budget in coastal
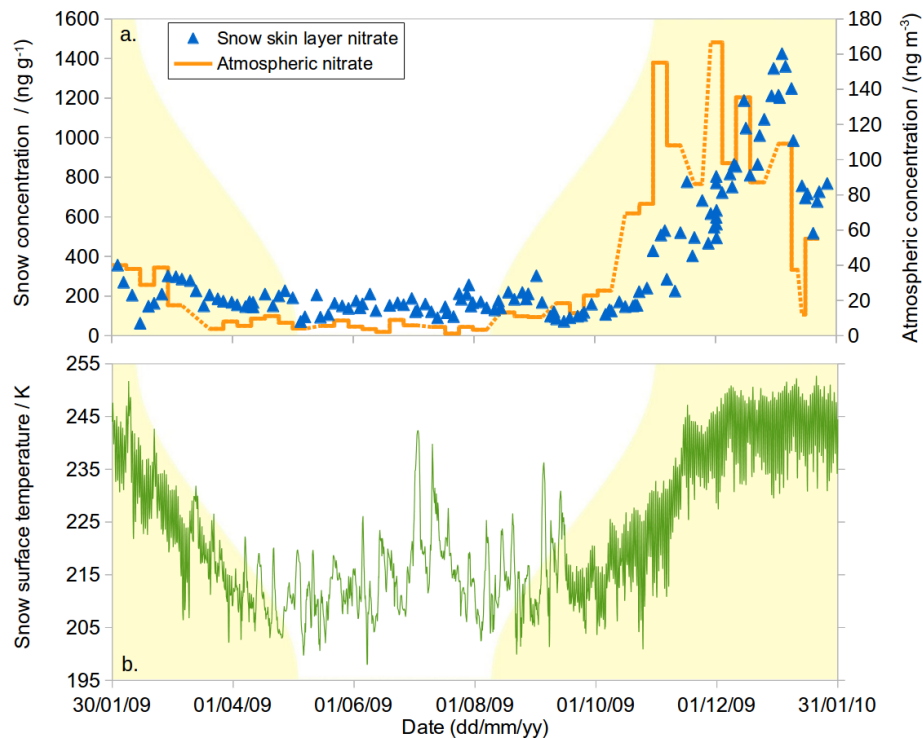
Antarctica and its link with surface snow and ice core nitrate: results from the CHABLIS campaign, Atmospheric Chemistry and Physics, 11, 9271–9285, doi:10.5194/acp-11-9271-2011, 2011.

Jones, A. E., Brough, N., Anderson, P. S., and Wolff, E. W.: HO_2NO_2 and HNO_3 in the coastal Antarctic winter night: a "lab-in-the-field" experiment, Atmospheric Chemistry and Physics, 14, 11 843–11 851, doi:10.5194/acp-14-11843-2014, 2014.

Kaempfer, T. and Plapp, M.: Phase-field modeling of dry snow metamorphism, Physical Review E, 79, 031 502, doi:10.1103/PhysRevE.79.031502, 2009.

Kärcher, B. and Basko, M. M.: Trapping of trace gases in growing ice crystals, Journal of Geophysical Research: Atmospheres, 109, D22 204, doi:10.1029/2004JD005254, 2004.

Kärcher, B., Abbatt, J. P. D., Cox, R. A., Popp, P. J., and Voigt, C.: Trapping of trace gases by growing ice surfaces including surface-saturated adsorption, Journal of Geophysical Research, 114, D13 306, doi:10.1029/2009JD011857, 2009.

Kerbrat, M., Huthwelker, T., Bartels-Rausch, T., Gäggeler, H. W., and Ammann, M.: Co-adsorption of acetic acid and nitrous acid on ice, Physical Chemistry Chemical Physics, 12, 7194–7202, doi:10.1039/b924782c, 2010.

Kuipers Munneke, P., van den Broeke, M. R., Reijmer, C. H., Helsen, M. M., Boot, W., Schneebeli, M., and Steffen, K.: The role of radiation penetration in the energy budget of the snowpack at Summit, Greenland, The Cryosphere, 3, 155–165, doi:10.5194/tc-3-155-2009, 2009.

Křepelová, A., Newberg, J., Huthwelker, T., Bluhm, H., and Ammann, M.: The nature of nitrate at the ice surface studied by XPS and NEXAFS, Physical Chemistry Chemical Physics, 12, 8870–8880, doi:10.1039/c0cp00359j, 2010.

Laird, S. K. and Sommerfeld, R. A.: Nitric acid adsorption on ice: a preliminary study, Geophysical Research Letters, 22, 921–923, doi:10.1029/95GL00817, 1995.

Legrand, M. and Mayewski, P.: Glaciochemistry of polar ice cores: a review, Reviews of Geophysics, 35, 219–243, doi:10.1029/96RG03527, 1997.

Leu, M.-T.: Laboratory studies of sticking coefficients and heterogeneous reactions important in the Antarctic stratosphere, Geophysical Research Letters, 15, 17–20, doi:10.1029/GL015i001p00017, 1988.

Leu, M.-T., Keyser, L. F., and Timonen, R. S.: Morphology and surface areas of thin ice films, The Journal of Physical Chemistry B, 101, 6259–6262, doi:10.1021/jp963251w, 1997.

Liao, W. and Tan, D.: 1-D Air-snowpack modeling of atmospheric nitrous acid at South Pole during ANTCI 2003, Atmospheric Chemistry and Physics, 8, 7087–7099, doi:10.5194/acp-8-7087-2008, 2008.

Libois, Q., Picard, G., Dumont, M., Arnaud, L., Sergent, C., Pougatch, E., Sudul, M., and Vial, D.: Experimental determination of the absorption enhancement parameter of snow, Journal of Glaciology, 60, 714–724, doi:10.3189/2014JoG14J015, 2014.

Libois, Q., Picard, G., Arnaud, L., Dumont, M., Lafaysse, M., Morin, S., and Lefebvre, E.: Summertime evolution of snow specific surface area close to the surface on the Antarctic Plateau, The Cryosphere, 9, 2383–2398, doi:10.5194/tc-9-2383-2015, 2015.

Marbouty, D.: An experimental study of temperature-gradient metamorphism, Journal of Glaciology, 26, 303–312, 1980.

1000   Marchand, P., Marcotte, G., and Ayotte, P.: Spectroscopic study of HNO_3 dissociation on ice, The Journal of Physical Chemistry A, 116, 12 112–12 122, doi:10.1021/jp309533f, 2012.

Marcotte, G., Ayotte, P., Bendounan, A., Sirotti, F., Laffon, C., and Parent, P.: Dissociative adsorption of nitric acid at the surface of amorphous solid water revealed by X-ray absorption spectroscopy, The Journal of Physical Chemistry Letters, 4, 2643–2648, doi:10.1021/jz401310j, 2013.

1005   Marcotte, G., Marchand, P., Pronovost, S., Ayotte, P., Laffon, C., and Parent, P.: Surface-enhanced nitrate photolysis on ice, The Journal of Physical Chemistry A, 119, 1996–2005, doi:10.1021/jp511173w, 2015.

McConnell, J. R., Bales, R. C., Winterle, J. R., Kuhns, H., and Stearns, C. R.: A lumped parameter model for the atmosphere-to-snow transfer function for hydrogen peroxide, Journal of Geophysical Research, 102, 26 809–26 818, doi:10.1029/96JC02194, 1997a.

1010   McConnell, J. R., Winterle, J. R., Bales, R. C., Thompson, A. M., and Stewart, R. W.: Physically based inversion of surface snow concentrations of H_2O_2 to atmospheric concentrations at South Pole, Geophysical Research Letters, 24, 441–444, doi:10.1029/97GL00183, 1997b.

McConnell, J. R., Bales, R. C., Stewart, R. W., Thompson, A. M., Albert, M. R., and Ramos, R.: Physically based modeling of atmosphere-to-snow-to-firn transfer of H_2O_2 at South Pole, Journal of Geophysical Re-
1015   search, 103, 10 561–10 570, doi:10.1029/98JD00460, 1998.

Meusinger, C., Berhanu, T. A., Erbland, J., Savarino, J., and Johnson, M. S.: Laboratory study of nitrate photolysis in Antarctic snow. I. Observed quantum yield, domain of photolysis, and secondary chemistry, The Journal of Chemical Physics, 140, 244 305, doi:10.1063/1.4882898, 2014.

Miller, D. and Adams, E.: A microstructural dry-snow metamorphism model for kinetic crystal growth, Journal
1020   of Glaciology, 55, 1003–1011, doi:10.3189/002214309790794832, 2009.

Murray, K. A., Kramer, L. J., Doskey, P. V., Ganzeveld, L., Seok, B., Van Dam, B., and Helmig, D.: Dynamics of ozone and nitrogen oxides at Summit, Greenland. II. Simulating snowpack chemistry during a spring high ozone event with a 1-D process-scale model, Atmospheric Environment, 117, 110–123, doi:10.1016/j.atmosenv.2015.07.004, 2015.

1025   Perrier, S., Sassin, P., and Dominé, F.: Diffusion and solubility of HCHO in ice: preliminary results, Canadian Journal of Physics, 81, 319–324, doi:10.1139/p03-033, 2003.

Picard, G., Brucker, L., Fily, M., Gallée, H., and Krinner, G.: Modeling time series of microwave brightness temperature in Antarctica, Journal of Glaciology, 55, 537–551, doi:10.3189/002214309788816678, 2009.

Picard, G., Domine, F., Krinner, G., Arnaud, L., and Lefebvre, E.: Inhibition of the positive snow-albedo feed-
1030   back by precipitation in interior Antarctica, Nature Climate Change, 2, 795–798, doi:10.1038/nclimate1590, 2012.

Pinzer, B. R. and Schneebeli, M.: Snow metamorphism under alternating temperature gradients: morphology and recrystallization in surface snow, Geophysical Research Letters, 36, L23 503, doi:10.1029/2009GL039618, 2009.

1035   Pinzer, B. R., Kerbrat, M., Huthwelker, T., Gäggeler, H. W., Schneebeli, M., and Ammann, M.: Diffusion of NO_x and HONO in snow: a laboratory study, Journal of Geophysical Research, 115, D03 304, doi:10.1029/2009JD012459, 2010.
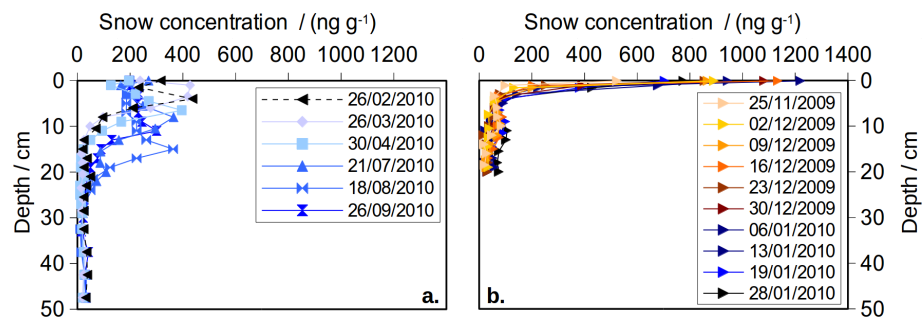
Pinzer, B. R., Schneebeli, M., and Kaempfer, T. U.: Vapor flux and recrystallization during dry snow metamorphism under a steady temperature gradient as observed by time-lapse micro-tomography, The Cryosphere, 6, 1141–1155, doi:10.5194/tc-6-1141-2012, 2012.

Preunkert, S., Ancellet, G., Legrand, M., Kukui, A., Kerbrat, M., Sarda-Estève, R., Gros, V., and Jourdain, B.: Oxidant Production over Antarctic Land and its Export (OPALE) project: an overview of the 2010–2011 summer campaign, Journal of Geophysical Research, 117, D15 307, doi:10.1029/2011JD017145, 2012.

Pruppacher, H. R. and Klett, J. D.: Microphysics of clouds and precipitation, Kluwer Academic Publishers, Dordrecht / Boston / London, 2nd revised and enlarged edn., 1997.

Riikonen, S., Parkkinen, P., Halonen, L., and Gerber, R. B.: Ionization of nitric acid on crystalline ice: the role of defects and collective proton movement, The Journal of Physical Chemistry Letters, 4, 1850–1855, doi:10.1021/jz400531q, 2013.

Riikonen, S., Parkkinen, P., Halonen, L., and Gerber, R. B.: Ionization of acids on the quasi-liquid layer of ice, The Journal of Physical Chemistry A, 118, 5029–5037, doi:10.1021/jp505627n, 2014.

Seinfeld, J. H. and Pandis, S. N.: Atmospheric chemistry and physics : from air pollution to climate change, Wiley, New York, 1998.

Sigg, A. and Neftel, A.: Seasonal variations in hydrogen peroxide in polar ice cores, Annals of Glaciology, 10, 157–162, 1988.

Sigg, A., Staffelbach, T., and Neftel, A.: Gas phase measurements of hydrogen peroxide in Greenland and their meaning for the interpretation of H_2O_2 records in ice cores, Journal of Atmospheric Chemistry, 14, 223–232, doi:10.1007/BF00115235, 1992.

Sokolov, O. and Abbatt, J. P. D.: Competitive adsorption of atmospheric trace gases onto ice at 228 K: HNO_3/HCl, 1-Butanol/Acetic acid and 1-Butanol/HCl, Geophysical Research Letters, 29, 1851, doi:10.1029/2002GL014843, 2002.

Sommerfeld, R. A.: A branch grain theory of temperature gradient metamorphism in snow, Journal of Geophysical Research, 88, 1484–1494, doi:10.1029/JC088iC02p01484, 1983.

Thibert, E. and Dominé, F.: Thermodynamics and kinetics of the solid solution of HCl in ice, The Journal of Physical Chemistry B, 101, 3554–3565, doi:10.1021/jp962115o, 1997.

Thibert, E. and Dominé, F.: Thermodynamics and kinetics of the solid solution of HNO_3 in ice, The Journal of Physical Chemistry B, 102, 4432–4439, doi:10.1021/jp980569a, 1998.

Thomas, J. L., Stutz, J., Lefer, B., Huey, L. G., Toyota, K., Dibb, J. E., and von Glasow, R.: Modeling chemistry in and above snow at Summit, Greenland – Part 1: model description and results, Atmospheric Chemistry and Physics, 11, 4899–4914, doi:10.5194/acp-11-4899-2011, 2011.

Town, M. S., Waddington, E. D., Walden, V. P., and Warren, S. G.: Temperatures, heating rates and vapour pressures in near-surface snow at the South Pole, Journal of Glaciology, 54, 487–498, doi:10.3189/002214308785837075, 2008.

Toyota, K., McConnell, J. C., Staebler, R. M., and Dastoor, A. P.: Air–snowpack exchange of bromine, ozone and mercury in the springtime Arctic simulated by the 1-D model PHANTAS – Part 1: in-snow bromine activation and its impact on ozone, Atmospheric Chemistry and Physics, 14, 4101–4133, doi:10.5194/acp-14-4101-2014, 2014.

Traversi, R., Usoskin, I. G., Solanki, S. K., Becagli, S., Frezzotti, M., Severi, M., Stenni, B., and Udisti, R.: Nitrate in polar ice: a new tracer of solar variability, Solar Physics, 280, 237–254, doi:10.1007/s11207-012-0060-3, 2012.

1080   Traversi, R., Udisti, R., Frosini, D., Becagli, S., Ciardini, V., Funke, B., Lanconelli, C., Petkov, B., Scarchilli, C., Severi, M., and Vitale, V.: Insights on nitrate sources at Dome C (East Antarctic Plateau) from multi-year aerosol and snow records, Tellus B, 66, 22 550, doi:10.3402/tellusb.v66.22550, 2014.

Ullerstam, M. and Abbatt, J. P. D.: Burial of gas-phase HNO_3 by growing ice surfaces under tropospheric conditions, Physical Chemistry Chemical Physics, 7, 3596–3600, doi:10.1039/b507797d, 2005.

1085   Ullerstam, M., Thornberry, T., and Abbatt, J. P. D.: Uptake of gas-phase nitric acid to ice at low partial pressures: evidence for unsaturated surface coverage, Faraday Discussions, 130, 211–226, doi:10.1039/b417418f, 2005.

Valdez, M. P., Dawson, G. A., and Bales, R. C.: Sulfur dioxide incorporation into ice depositing from the vapor, Journal of Geophysical Research, 94, 1095–1103, doi:10.1029/JD094iD01p01095, 1989.

Wolff, E. W., Jones, A. E., Bauguitte, S. J.-B., and Salmon, R. A.: The interpretation of spikes and trends in

1090   concentration of nitrate in polar ice cores, based on evidence from snow and atmospheric measurements, Atmospheric Chemistry and Physics, 8, 5627–5634, doi:10.5194/acp-8-5627-2008, 2008.

Xueref, I. and Dominé, F.: FTIR spectroscopic studies of the simultaneous condensation of HCl and H_2O at 190 K – Atmospheric applications, Atmospheric Chemistry and Physics, 3, 1779–1789, doi:10.5194/acp-3-1779-2003, 2003.

1095   Zhu, C., Xiang, B., Chu, L. T., and Zhu, L.: 308 nm photolysis of nitric acid in the gas phase, on aluminum surfaces, and on ice films, The Journal of Physical Chemistry A, 114, 2561–2568, doi:10.1021/jp909867a, 2010.

Zondlo, M. A., Barone, S. B., and Tolbert, M. A.: Uptake of HNO_3 on ice under upper tropospheric conditions, Geophysical Research Letters, 24, 1391–1394, doi:10.1029/97GL01287, 1997.
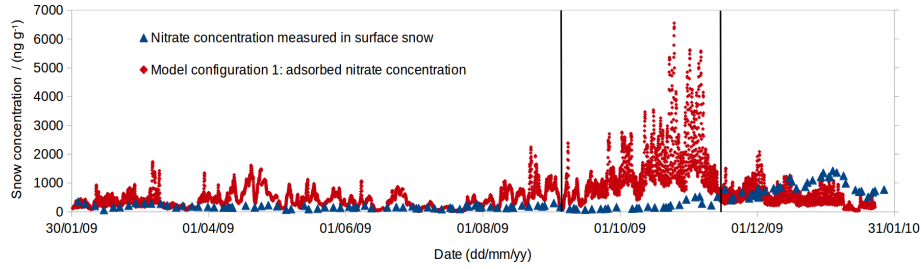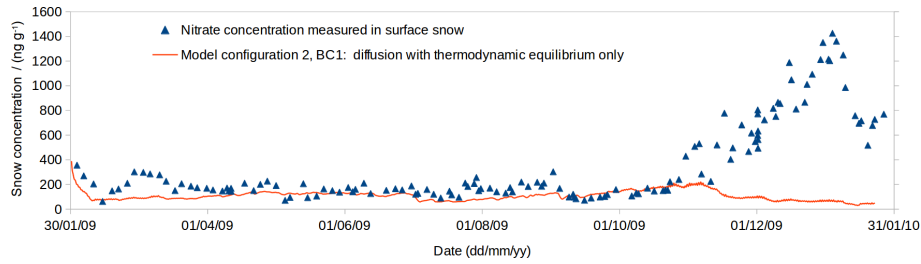
Figure 1. (a) Atmospheric nitrate concentration (orange lines, right axis) and snow skin layer nitrate concentration (blue triangles, left axis). **(b)** Modelled surface snow temperature. In both panels, the back yellow coloured area is proportional to sunlight duration.
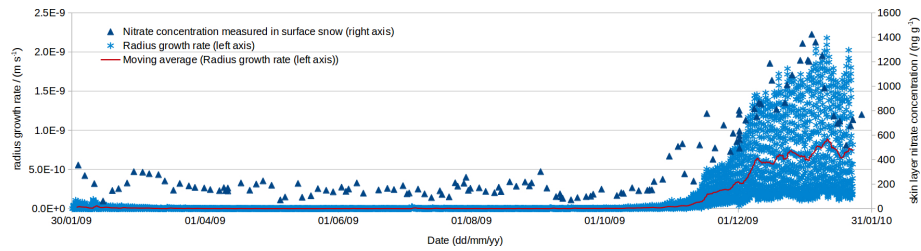

Figure 2. (a) Winter nitrate concentration profiles (in ng g^{-1}) in snow pits. **(b)** Summer nitrate concentration profiles (in ng g^{-1}). The measurement date (dd/mm/yyyy) is indicated.
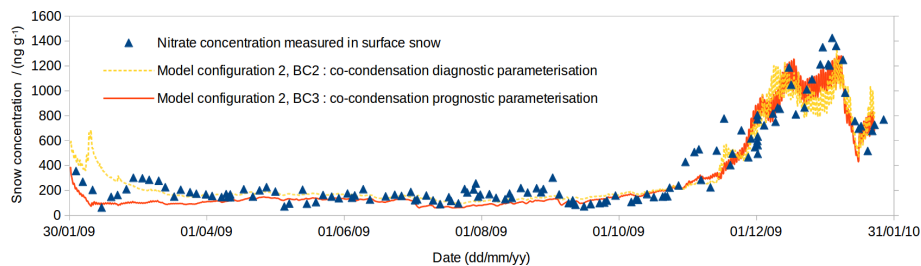
Figure 3. Concentration of nitrate in snow skin layer: measured concentration (blue triangles) and model configuration 1: adsorbed concentration (red diamonds). Note the y-axis scale change as compared to Fig. 1a. The output timestep is one hour. Verticals bars are visual aids to separate periods mentioned in the text.

Figure 4. Nitrate concentration in the skin layer: measured concentrations (blue triangles) and model configuration 2 (orange line) using only thermodynamic solubility to constrain the air–snow partitioning (BC1). The output timestep is 4 hours.

Figure 5. Radius growth rate calculated according to Eq. (14). Hourly data (blue asterisks) is plotted along with a moving average (red line). Nitrate concentration in the skin layer (blue triangles, right axis) is plotted for a comparison of both yearly patterns.

34

Figure 6. Nitrate concentration in the skin layer: measured concentrations (blue triangles) and mode configuration 2 using two distinct parameterisations of the co-condensation process: diagnostic parameterisation (BC2, dashed yellow line) and physically based prognostic parameterisation (BC3, solid red line).

Table 1. Summary of the main simulations with their description, along with the RMSE value to evaluate the discrepancy between modelled and measured values. If relevant, the numbering of the figure where results are plotted is indicated.

Simulation description	RMSE / ng g^{-1}	Fig.
Configuration 1: adsorption	551	3
Configuration 2: diffusion with thermodynamic solubility only (BC1)	437	4
Configuration 2: diffusion with diagnostic parametrisation of the co-condensation (BC2)	124	6
Configuration 2: diffusion with prognostic parameterisation of the co-condensation (BC3)	116	6
Sensitivity study, solubility increased by 39 %	110	
Sensitivity study, diffusion coefficient decreased by 72 %	100	
Sensitivity study, solubility increased by 39 % and diffusion coefficient decreased by 64 %	96	
Sensitivity study, solubility increased by 39 % and SSA value decreased to 23 m^2 kg^{-1} (initial value = 38 m^2 kg^{-1})	96	